





**TABLE 65.1** Material Properties of Linear-Array Elements Made of PZT-5H

| Parameter                              | Symbol                | Value | Units             |
|--|-----------------------|-------|-------------------|
| Density                                | $\rho$                | 7500  | kg/m <sup>3</sup> |
| Speed of sound                         | $c$                   | 3970  | m/s               |
| Acoustic impedance                     | $Z$                   | 29.75 | MRayls            |
| Relative dielectric constant           | $\epsilon/\epsilon_0$ | 1475  | None              |
| Electromechanical coupling coefficient | $k$                   | 0.698 | None              |
| Mechanical loss tangent                | $\tan \delta_m$       | 0.015 | None              |
| Electrical loss tangent                | $\tan \delta_e$       | 0.02  | None              |

### Transducer Materials

Ferroelectric materials strongly exhibit the piezoelectric effect, and they are ideal materials for medical ultrasound. For many years, the ferroelectric ceramic lead-zirconate-titanate (PZT) has been the standard transducer material for medical ultrasound, in part because of its high electromechanical conversion efficiency and low intrinsic losses. The properties of PZT can be adjusted by modifying the ratio of zirconium to titanium and introducing small amounts of other substances, such as lanthanum [Berlincourt, 1971]. Table 65.1 shows the material properties of linear-array elements made from PZT-5H.

PZT has a high dielectric constant compared with many piezoelectric materials, resulting in favorable electrical characteristics. The ceramic is mechanically strong, and it can be machined to various shapes and sizes. PZT can operate at temperatures up to 100°C or higher, and it is stable over long periods of time.

The disadvantages of PZT include its high acoustic impedance ( $Z = 30$  MRayls) compared with body tissue ( $Z = 1.5$  MRayls) and the presence of lateral modes in array elements. One or more acoustic matching layers can largely compensate for the acoustic impedance mismatch. The effect of lateral modes can be diminished by choosing the appropriate element dimensions or by subdicing the elements.

Other piezoelectric materials are used for various applications. Composites are made from PZT interspersed in an epoxy matrix [Smith, 1992]. Lateral modes are reduced in a composite because of its inhomogeneous structure. By combining the PZT and epoxy in different ratios and spatial distributions, one can tailor the composite's properties for different applications. Polyvinylidene difluoride (PVDF) is a ferroelectric polymer that has been used effectively in high-frequency transducers [Sherar and Foster, 1989]. The copolymer of PVDF with trifluoroethylene has an improved electromechanical conversion efficiency. Relaxor ferroelectric materials, such as lead-magnesium-niobate (PMN), become piezoelectric when a large direct-current (dc) bias voltage is applied [Takeuchi et al., 1990]. They have a very large dielectric constant ( $\epsilon > 20,000\epsilon_0$ ), resulting in higher transducer capacitance and a lower electrical impedance.

### Scanning with Array Transducers

Array transducers use the same principles as acoustic lenses to focus an acoustic beam. In both cases, variable delays are applied across the transducer aperture. With a sequential or phased array, however, the delays are electronically controlled and can be changed instantaneously to focus the beam in different regions. Linear arrays were first developed for radar, sonar, and radio astronomy [Allen, 1964; Bobber, 1970], and they were implemented in a medical ultrasound system by Somer in 1968 [Somer, 1968].

Linear-array transducers have increased versatility over piston transducers. Electronic scanning involves no moving parts, and the focal point can be changed dynamically to any location in the scanning plane. The system can generate a wide variety of scan formats, and it can process the received echoes for other applications, such as dynamic receive focusing [von Ramm and Thurstone, 1976], correction for phase aberrations [Flax and O'Donnell, 1988; Trahey et al., 1990], and synthetic aperture imaging [Nock and Trahey, 1992].

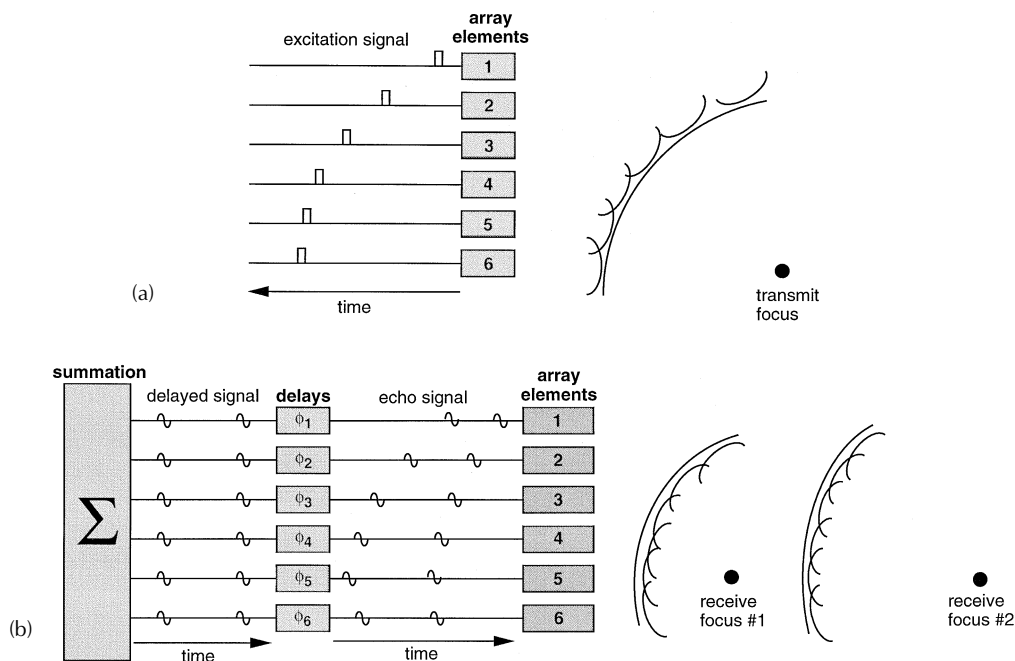


**FIGURE 65.1** Focusing and steering an acoustic beam using a phased array. A 6-element linear array is shown (a) in the transmit mode and (b) in the receive mode. Dynamic focusing in receive allows the scanner focus to track the range of returning echoes.

The disadvantages of linear arrays are due to the increased complexity and higher cost of the transducers and scanners. For high-quality ultrasound images, many identical array elements are required (currently 128 and rising). The array elements are typically less than a millimeter on one side, and each has a separate connection to its own transmitter and receiver electronics.

The widespread use of array transducers for many applications indicates that the advantages often outweigh the disadvantages. In addition, improvement in transducer fabrication techniques and integrated circuit technology have led to more advanced array transducers and scanners.

### Focusing and Steering with Phased Arrays

This subsection describes how a phased-array transducer can focus and steer an acoustic beam along a specific direction. An ultrasound image is formed by repeating this process over 100 times to interrogate a two- (2D) or three-dimensional (3D) region of the medium.

Figure 65.1a illustrates a simple example of a six-element linear array focusing the transmitted beam. One can assume that each array element is a point source that radiates a spherically shaped wavefront into the medium. Since the top element is farthest from the focus in this example, it is excited first. The remaining elements are excited at the appropriate time intervals so that the acoustic signals from all the elements reach the focal point at the same time. According to Huygens' principle, the net acoustic signal is the sum of the signals that have arrived from each source. At the focal point, the contributions from every element add in phase to produce a peak in the acoustic signal. Elsewhere, at least some of the contributions add out of phase, reducing the signal relative to the peak.

For receiving an ultrasound echo, the phased array works in reverse. Fig. 65.1b shows an echo originating from focus 1. The echo is incident on each array element at a different time interval. The received signals are electronically delayed so that the delayed signals add in phase for an echo originating at the focal point. For echoes originating elsewhere, at least some of the delayed signals will add out of phase, reducing the receive signal relative to the peak at the focus.

In the receive mode, the focal point can be dynamically adjusted so that it coincides with the range of returning echoes. After transmission of an acoustic pulse, the initial echoes return from targets near the transducer. Therefore, the scanner focuses the phased array on these targets, located at focus 1 in Fig. 65.1b. As echoes return from more distant targets, the scanner focuses at a greater depth (focus 2 in the figure). Focal zones are established with adequate depth of field so that the targets are always in focus in receive. This process is called *dynamic receive focusing* and was first implemented by von Ramm and Thurstone in 1976 [von Ramm and Thurstone, 1976].

### Array-Element Configurations

An ultrasound image is formed by repeating the preceding process many times to scan a 2D or 3D region of tissue. For a 2D image, the scanning plane is the **azimuth dimension**; the **elevation dimension** is perpendicular to the azimuth scanning plane. The shape of the region scanned is determined by the array-element configuration, described in the paragraph below.

**Linear Sequential Arrays.** Sequential linear arrays have as many as 512 elements in current commercial scanners. A subaperture of up to 128 elements is selected to operate at a given time. As shown in Fig. 65.2a, the scanning lines are directed perpendicular to the face of the transducer; the acoustic beam is focused but not steered. The advantage of this scheme is that the array elements have high sensitivity when the beam is directed straight ahead. The disadvantage is that the field of view is limited to the rectangular region directly in front of the transducer. Linear-array transducers have a large footprint to obtain an adequate field of view.

**Curvilinear Arrays.** Curvilinear or convex arrays have a different shape than sequential linear arrays, but they operate in the same manner. In both cases, the scan lines are directed perpendicular to the transducer face. A curvilinear array, however, scans a wider field of view because of its convex shape, as shown in Fig. 65.2b.

**Linear Phased Arrays.** The more advanced linear phased arrays have 128 elements. All the elements are used to transmit and receive each line of data. As shown in Fig. 65.2c, the scanner steers the ultrasound beam through a sector-shaped region in the azimuth plane. Phased arrays scan a region that is significantly wider than the footprint of the transducer, making them suitable for scanning through restricted acoustic windows. As a result, these transducers are ideal for cardiac imaging, where the transducer must scan through a small window to avoid the obstructions of the ribs (bone) and lungs (air).

**1.5D Arrays.** The so-called 1.5D array is similar to a 2D array in construction but a 1D array in operation. The 1.5D array contains elements along both the azimuth and elevation dimensions. Features such dynamic focusing and phase correction can be implemented in both dimensions to improve image quality. Since a 1.5D array contains a limited number of elements in elevation (e.g., 3 to 9 elements), steering is not possible in that direction. Figure 65.2d illustrates a B-scan made with a 1.5D phased array. Linear sequential scanning is also possible with 1.5D arrays.

**2D Phased Arrays.** A 2D phased-array has a large number of elements in both the azimuth and elevation dimensions. Therefore, 2D arrays can focus and steer the acoustic beam in both dimensions. Using parallel receive processing [Shattuck et al., 1984], a 2D array can scan a pyramidal region in real time to produce a volumetric image, as shown in Fig. 65.2e [von Ramm and Smith, 1990].

### Linear-Array Transducer Performance

Designing an ultrasound transducer array involves many compromises. Ideally, a transducer has high sensitivity or SNR, good spatial resolution, and no artifacts. The individual array elements should have wide angular response in the steering dimensions, low cross-coupling, and an electrical impedance matched to the transmitter.

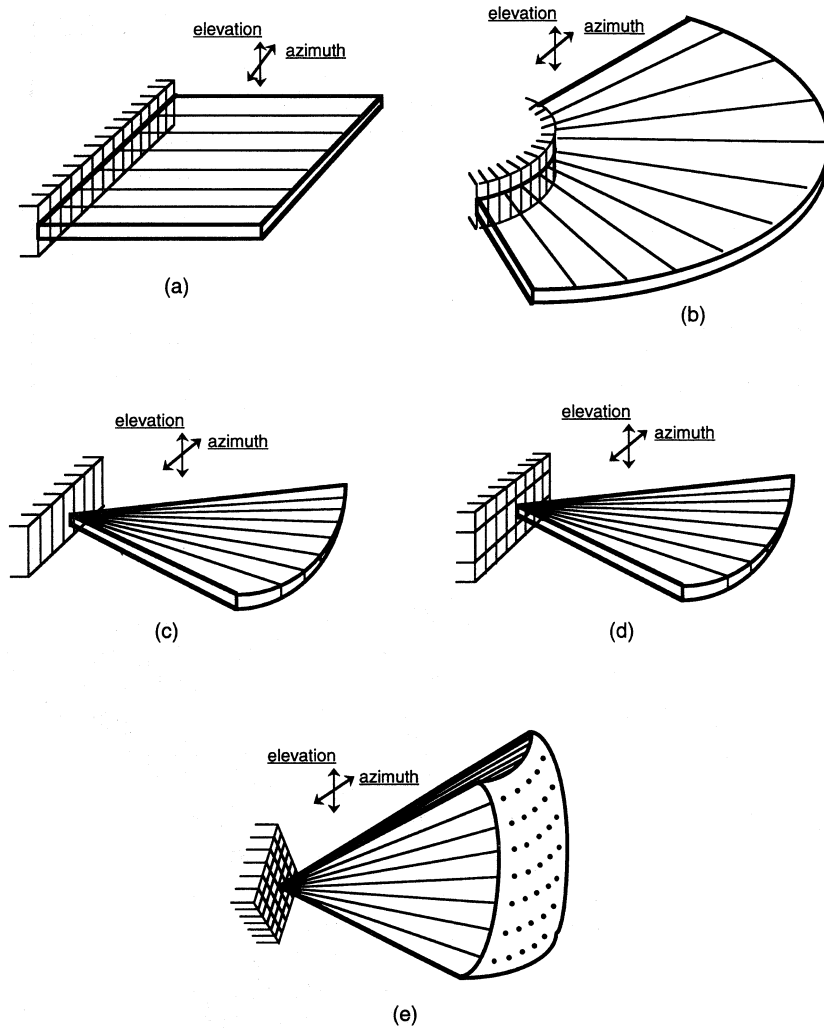


**FIGURE 65.2** Array-element configurations and the region scanned by the acoustic beam. (a) A sequential linear array scans a rectangular region; (b) a curvilinear array scans a sector-shaped region; (c) a linear phased array scans a sector-shaped region; (d) a 1.5D array scans a sector-shaped region; (e) a 2D array scans a pyramidal-shaped region.

Figure 65.3a illustrates the connections to the transducer assembly. The transmitter and receiver circuits are located in the ultrasound scanner and are connected to the array elements through 1 to 2 m of coaxial cable. Electrical matching networks can be added to tune out the capacitance of the coaxial cable and/or the transducer element and increase the signal-to-noise ratio (SNR).

A more detailed picture of six-transducer elements is shown in Fig. 65.3b. Electrically, the array elements are loaded on the front side by one or two quarter-wave matching layers and the tissue medium. The matching layers may be made from glass or epoxy. A backing material, such as epoxy, loads the back side of the array elements. The faceplate protects the transducer assembly and also may act as an acoustic lens. Faceplates are often made from silicone or polyurethane.

The following subsections describe several important characteristics of an array transducer. Figure 65.3c shows a six-element array and its dimensions. The element thickness, width, and length are labeled as  $t$ ,  $a$ , and  $b$ , respectively. The interelement spacing is  $d$ , and the total aperture size is  $D$  in

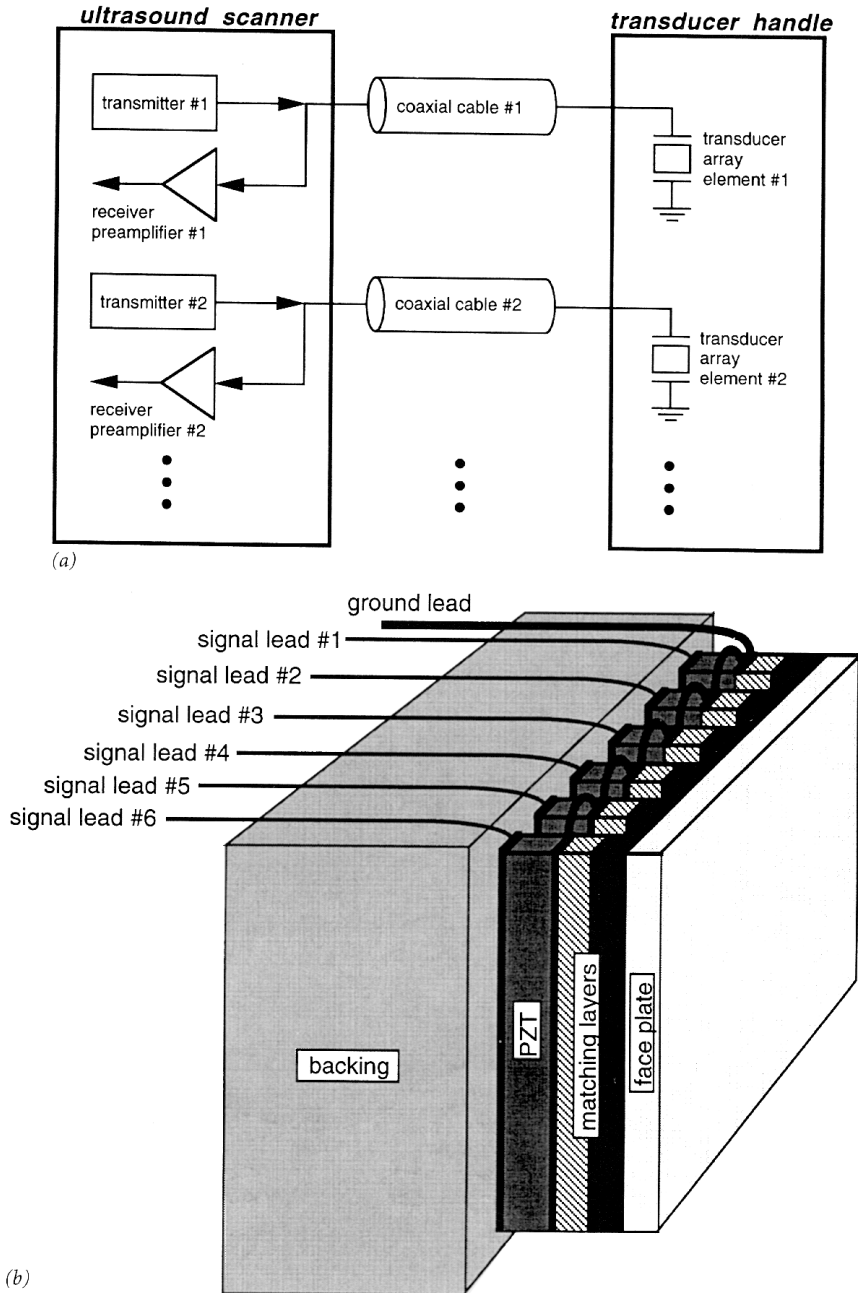


**FIGURE 65.3** (a) The connections between the ultrasound scanner and the transducer assembly for two elements of an array. (b) A more detailed picture of the transducer assembly for six elements of an array. (c) Coordinate system and labeling used to describe an array transducer.

azimuth. The acoustic wavelength in the load medium, usually human tissue, is designated as  $\lambda$ , while the wavelength in the transducer material is  $\lambda_t$ .

Examples are given below for a 128-element linear array operating at 5 MHz. The array is made of PZT-5H with element dimensions of  $0.1 \times 5 \times 0.3$  mm. The interelement spacing is  $d = 0.15$  mm in

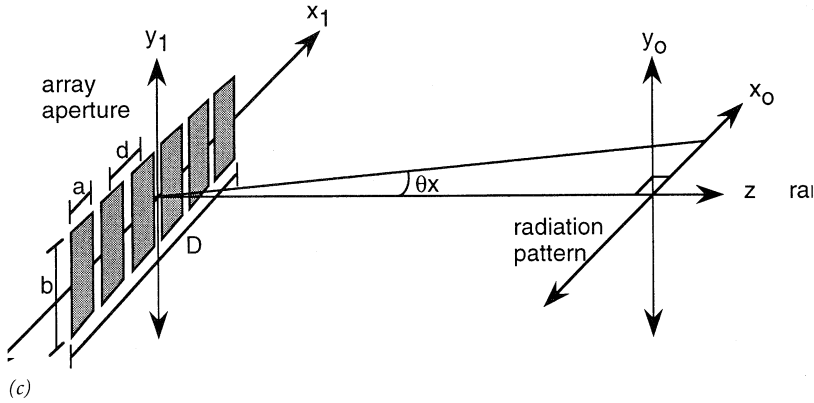


FIGURE 65.3 (continued)

azimuth, and the total aperture is  $D = 128 \cdot 0.15 \text{ mm} = 19.3 \text{ mm}$ . See Table 65.1 for the piezoelectric material characteristics. The elements have an epoxy backing of  $Z = 3.25 \text{ MRayls}$ . For simplicity, the example array does not contain a  $\lambda/4$  matching layer.

### Axial Resolution

**Axial resolution** determines the ability to distinguish between targets aligned in the axial direction (the direction of acoustic propagation). In pulse-echo imaging, the echoes off of two targets separated by  $r/2$  have a path length difference of  $r$ . If the acoustic pulse length is  $r$ , then echoes off the two targets are just distinguishable. As a result, the axial resolution is often defined as one-half the pulse length [Christensen, 1988]. A transducer with a high resonant frequency and a broad bandwidth has a short acoustic pulse and good axial resolution.

### Radiation Pattern

The radiation pattern of a transducer determines the insonified region of tissue. For good lateral resolution and sensitivity, the acoustic energy should be concentrated in a small region. The radiation pattern for a narrow-band or continuous-wave (CW) transducer is described by the Rayleigh-Sommerfeld diffraction formula [Goodman, 1986]. For a pulse-echo imaging system, this diffraction formula is not exact due to the broadband acoustic waves used. Nevertheless, the Rayleigh-Sommerfeld formula is a reasonable first-order approximation to the actual radiation pattern.

The following analysis considers only the azimuth scanning dimension. Near the focal point or in the far field, the Fraunhofer approximation reduces the diffraction formula to a Fourier transform formula. For a circular or rectangular aperture, the far field is at a range of

$$z > \frac{D^2}{4\lambda} \quad (65.1)$$

Figure 65.3c shows the coordinate system used to label the array aperture and its radiation pattern. The array aperture is described by

$$\text{Array}(x_1) = \text{rect}\left(\frac{x_1}{a}\right) * \text{comb}\left(\frac{x_1}{d}\right) \cdot \text{rect}\left(\frac{x_1}{D}\right) \quad (65.2)$$

where the  $\text{rect}(x)$  function is a rectangular pulse of width  $x$ , and the  $\text{comb}(x)$  function is a delta function repeated at intervals of  $x$ . The diffraction pattern is evaluated in the  $x_0$  plane at a distance  $z$  from the



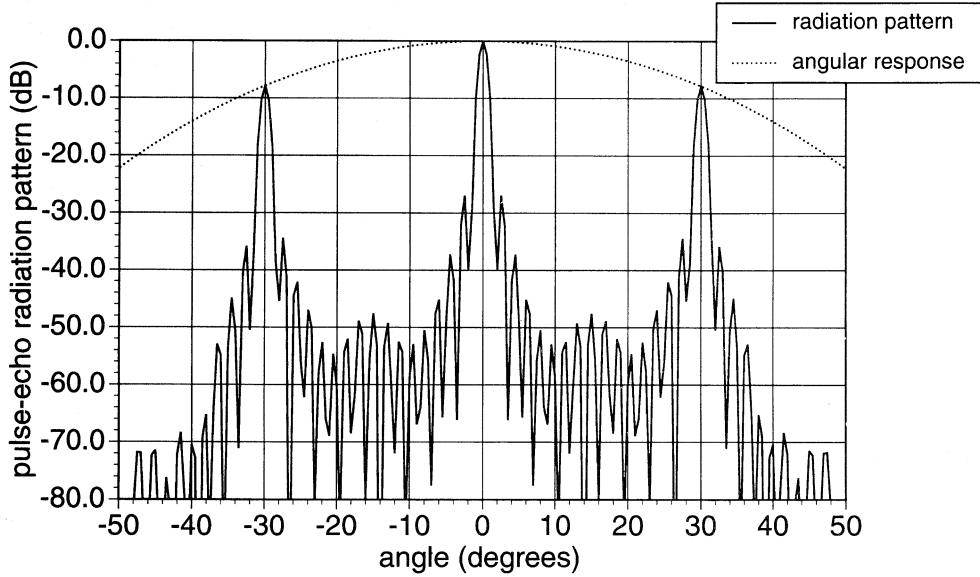


FIGURE 65.4 Radiation pattern of Eq. (65.3) for a 16-element array with  $a = \lambda$ ,  $d = 2\lambda$ , and  $D = 32\lambda$ . The angular response, the first term of Eq. (65.3), is also shown as a dashed line.

transducer, and  $\theta_x$  is the angle of the point  $x_0$  from the normal axis. With the Fraunhofer approximation, the normalized diffraction pattern is given by

$$P_x(\theta_x) = \text{sinc}\left(\frac{a \sin \theta_x}{\lambda}\right) \cdot \text{comb}\left(\frac{d \sin \theta_x}{\lambda}\right) * \text{sinc}\left(\frac{D \sin \theta_x}{\lambda}\right) \quad (65.3)$$

in azimuth, where the Fourier transform of Eq. (65.2) has been evaluated at the spatial frequency

$$f_x = \frac{x_0}{\lambda z} = \frac{\sin \theta_x}{\lambda} \quad (65.4)$$

Figure 65.4 shows a graph of Eq. (65.3) for a 16-element array with  $a = \lambda$ ,  $d = 2\lambda$ , and  $D = 32\lambda$ . In the graph, the significance of each term is easily distinguished. The first term determines the angular response weighting, the second term determines the location of grating lobes off-axis, and the third term determines the shape of the main lobe and the grating lobes. The significance of **lateral resolution**, **angular response**, and **grating lobes** is seen from the CW diffraction pattern.

Lateral resolution determines the ability to distinguish between targets in the azimuth and elevation dimensions. According to the Rayleigh criterion [Goodman, 1986], the *lateral resolution* can be defined by the first null in the main lobe, which is determined from the third term of Eq. (65.3).

$$\theta_x = \sin^{-1} \frac{\lambda}{D} \quad (65.5)$$

in the azimuth dimension. A larger aperture results in a more narrow main lobe and better resolution.

A broad angular response is desired to maintain sensitivity while steering off-axis. The first term of Eq. (65.3) determines the one-way angular response. The element is usually surrounded by a soft baffle,

such as air, resulting in an additional cosine factor in the radiation pattern [Selfridge et al., 1980]. Assuming transmit/receive reciprocity, the pulse-echo angular response for a single element is

$$P_x(\theta_x) = \frac{\sin^2(\pi a/\lambda \cdot \sin \theta_x)}{(\pi a/\lambda \cdot \sin \theta_x)^2} \cdot \cos^2 \theta_x \quad (65.6)$$

in the azimuth dimension. As the aperture size becomes smaller, the element more closely resembles a point source, and the angular response becomes more broad. Another useful indicator is the  $-6$ -dB angular response, defined as the full-width half-maximum of the angular response graph.

Grating lobes are produced at a location where the path length difference to adjacent array elements is a multiple of a wavelength (the main lobe is located where the path length difference is zero). The acoustic contributions from the elements constructively interfere, producing off-axis peaks. The term *grating lobe* was originally used to describe the optical peaks produced by a diffraction grating. In ultrasound, grating lobes are undesirable because they represent acoustic energy steered away from the main lobe. From the Comb function in Eq. (65.3), the grating lobes are located at

$$\theta_x = \sin^{-1} \frac{i\lambda}{d} \quad i = 1, 2, 3, \dots \quad (65.7)$$

in azimuth.

If  $d$  is a wavelength, then grating lobes are centered at  $\pm 90$  degrees from the steering direction in that dimension. Grating lobes at such large angles are less significant because the array elements have poor angular response in those regions. If the main lobe is steered at a large angle, however, the grating lobes are brought toward the front of the array. In this case, the angular response weighting produces a relatively weak main lobe and a relatively strong grating lobe. To eliminate grating lobes at all steering angles, the interelement spacing is set to  $\lambda/2$  or less [Steinberg, 1967].

Figure 65.5 shows the theoretical radiation pattern of the 128-element example. For this graph, the angular response weighting of Eq. (65.6) was substituted into Eq. (65.3). The lateral resolution, as defined by Eq. (65.7),  $\theta_x = 0.9$  degrees at the focal point. The  $-6$ -dB angular response is  $\pm 40$  degrees from Eq. (65.6).

## Electrical Impedance

The electric impedance of an element relative to the electrical loads has a significant impact on transducer signal-to-noise ratio (SNR). At frequencies away from resonance, the transducer has electrical characteristics of a capacitor. The construction of the transducer is a parallel-plate capacitor with clamped capacitance of

$$C_0 = \epsilon^s \frac{ab}{t} \quad (65.8)$$

where  $\epsilon^s$  is the clamped dielectric constant.

Near resonance, equivalent circuits help to explain the impedance behavior of a transducer. The simplified circuit of Fig. 65.6a is valid for transducers operating at series resonance without losses and with low acoustic impedance loads [Kino, 1987]. The mechanical resistance  $R_m$  represents the acoustic loads as seen from the electrical terminals:

$$R_m = \frac{\pi}{4k^2 \omega C_0} \cdot \frac{Z_1 + Z_2}{Z_c} \quad (65.9)$$

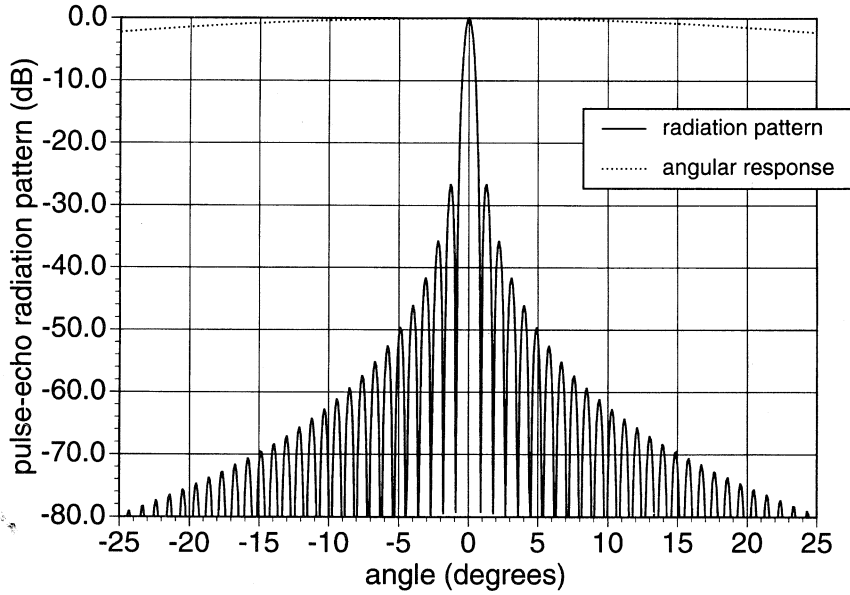


**FIGURE 65.5.** Radiation pattern of the example array element with  $a = 0.1$  mm,  $d = 0.15$  mm,  $D = 19.2$  mm, and  $\lambda = 0.3$  mm. The angular response of Eq. (65.6) was substituted into Eq. (65.3) for this graph.

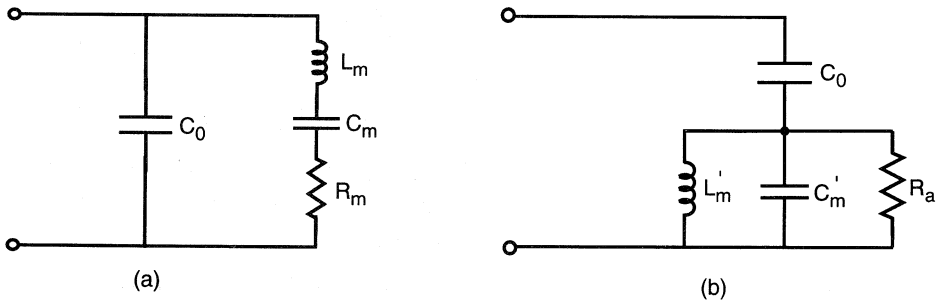


**FIGURE 65.6** Simplified equivalent circuits for a piezoelectric transducer: (a) near-series resonance and (b) near-parallel resonance.

where  $k$  is the electromechanical coupling coefficient of the piezoelectric material,  $Z_C$  is the acoustic impedance of the piezoelectric material,  $Z_1$  is the acoustic impedance of the transducer backing, and  $Z_2$  is the acoustic impedance of the load medium (body tissue). The power dissipated through  $R_m$  corresponds to the acoustic output power from the transducer.

The mechanical inductance  $L_m$  and mechanical capacitance  $C_m$  are analogous to the inductance and capacitance of a mass-spring system. At the series resonant frequency of

$$f_s = \frac{1}{2\pi\sqrt{L_m C_m}} \quad (65.10)$$

the impedances of these components add to zero, resulting in a local impedance minimum.

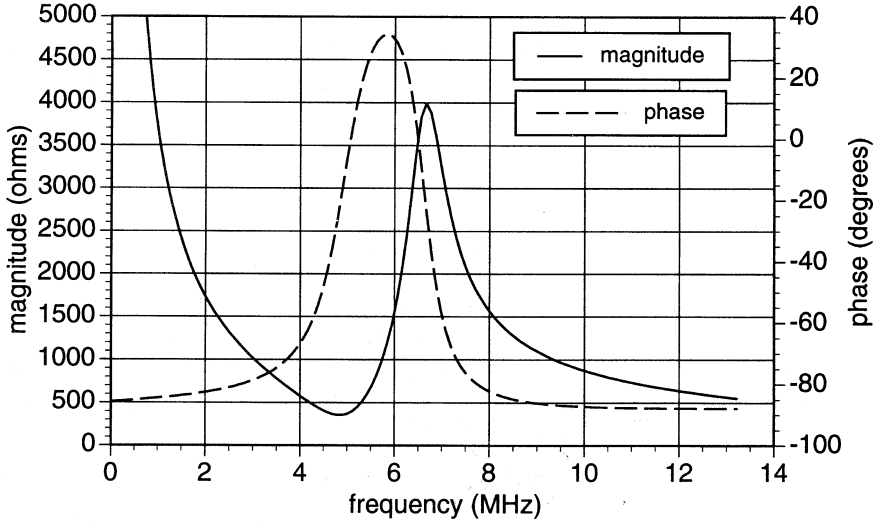


**FIGURE 65.7** Complex electrical impedance of the example array element. Series resonance is located at 5.0 MHz, and parallel resonance is located at 6.7 MHz.

The equivalent circuit of Fig. 65.6a can be redrawn in the form shown in Fig. 65.6b. In this circuit,  $C_0$  is the same as before, but the mechanical impedances have values of  $L'_m$ ,  $C'_m$ , and  $R_a$ . The resistive component  $R_a$  is

$$R_a = \frac{4k^2}{\pi\omega C_0} \cdot \frac{Z_c}{Z_1 + Z_2} \quad (65.11)$$

The inductor and capacitor combine to form an open circuit at the parallel resonant frequency of

$$f_p = \frac{1}{2\pi\sqrt{L'_m C'_m}} \quad (65.12)$$

The parallel resonance, which is at a slightly higher frequency than the series resonance, is indicated by a local impedance maximum.

Figure 65.7 shows a simulated plot of magnitude and phase versus frequency for the example array element described at the beginning of this subsection. The series resonance frequency is immediately identified at 5.0 MHz with an impedance minimum of  $|Z| = 350 \Omega$ . Parallel resonance occurs at 6.7 MHz with an impedance maximum of  $|Z| = 4000 \Omega$ . Note the capacitive behavior (approximately  $-90$ -degree phase) at frequencies far from resonance.

## Designing a Phased-Array Transducer

In this subsection the design of an idealized phased-array transducer is considered in terms of the performance characteristics described above. Criteria are described for selecting array dimensions, acoustic backing and matching layers, and electrical matching networks.

### Choosing Array Dimensions

The array element thickness is determined by the parallel resonant frequency. For  $\lambda/2$  resonance, the thickness is

$$t = \frac{\lambda_t}{2} = \frac{c_t}{2f_p} \quad (65.13)$$

where  $c_t$  is the longitudinal speed of sound in the transducer material.

There are three constraints for choosing the element width and length: (1) a nearly square cross-section should be avoided so that lateral vibrations are not coupled to the thickness vibration; as a rule of thumb [Kino and DeSilets, 1979],

$$a/t \leq 0.6 \quad \text{or} \quad a/t \geq 10 \quad (65.14)$$

(2) a small width and length are also desirable for a wide angular response weighting function; and (3) an interelement spacing of  $\lambda/2$  or less is necessary to eliminate grating lobes.

Fortunately, these requirements are consistent for PZT array elements. For all forms of PZT,  $c_t > 2c$ , where  $c$  is the speed of sound in body tissue (an average of 1540 m/s). At a given frequency, then  $\lambda_t > 2\lambda$ . Also, Eq. (65.13) states that  $\lambda_t = 2t$  at a frequency of  $f_p$ . By combining these equations,  $t > \lambda$  for PZT array elements operating at a frequency of  $f_p$ . If  $d = \lambda/2$ , then  $a < \lambda/2$  because of the finite kerf width that separates the elements. Given this observation, then  $a < t/2$ . This is consistent with Eq. (65.14) to reduce lateral modes.

An element having  $d = \lambda/2$  also has adequate angular response. For illustrative purposes, one can assume a zero kerf width so that  $a = \lambda/2$ . In this case, the  $-6$ -dB angular response is  $\theta_x = \pm 35$  degrees according to Eq. (65.6).

The array dimensions determine the transducer's lateral resolution. In the azimuth dimension, if  $d = \lambda/2$ , then the transducer aperture is  $D = n\lambda/2$ , where  $n$  is the number of elements in a fully sampled array. From Eq. (65.5), the lateral resolution in azimuth is

$$\theta_x = \sin^{-1} \frac{2}{n} \quad (65.15)$$

Therefore, the lateral resolution is independent of frequency in a fully sampled array with  $d = \lambda/2$ . For this configuration, the lateral resolution is improved by increasing the number of elements.

### Acoustic Backing and Matching Layers

The backing and matching layers affect the transducer bandwidth and sensitivity. While a lossy, matched backing improves bandwidth, it also dissipates acoustic energy that could otherwise be transmitted into the tissue medium. Therefore, a low-impedance acoustic backing is preferred because it reflects the acoustic pulses toward the front side of the transducer. In this case, adequate bandwidth is maintained by acoustically matching the transducer to the tissue medium using matching layers.

Matching layers are designed with a thickness of  $\lambda/4$  at the center frequency and an acoustic impedance between those of the transducer  $Z_T$  and the load medium  $Z_L$ . The ideal acoustic impedances can be determined from several different models [Hunt et al., 1983]. Using the KLM equivalent circuit model [Desilets et al., 1978], the ideal acoustic impedance is

$$Z_1 = \sqrt[3]{Z_T Z_L^2} \quad (65.16)$$

for a single matching layer. For matching PZT-5H array elements ( $Z_T = 30$  MRays) to a water load ( $Z_L = 1.5$  MRays), a matching layer of  $Z_1 = 4.1$  MRays should be chosen. If two matching layers are used, they should have acoustic impedances of

$$Z_1 = \sqrt[7]{Z_T^4 Z_L^3} \quad (65.17a)$$

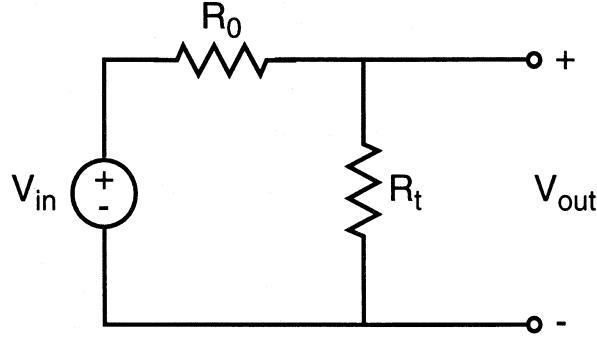


**FIGURE 65.8** A transducer of real impedance  $R_t$  being excited by a transmitter with source impedance  $R_0$  and source voltage  $V_{in}$ .

$$Z_2 = \sqrt[7]{Z_T Z_L^6} \quad (65.17b)$$

In this case,  $Z_1 = 8.3$  MRayls and  $Z_2 = 2.3$  MRayls for matching PZT-5H to a water load.

When constructing a transducer, a practical matching layer material is not always available, with the ideal acoustic impedance [Eq. (65.16) or (65.17)]. Adequate bandwidth is obtained by using materials that have an impedance close to the ideal value. With a single matching layer, for example, conductive epoxy can be used with  $Z = 5.1$  MRayls.

### Electrical Impedance Matching

Signal-to-noise ratio and bandwidth are also improved when electrical impedance of an array element is matched to that of the transmit circuitry. Consider the simplified circuit in Fig. 65.8 with a transmitter of impedance  $R_0$  and a transducer of real impedance  $R_t$ . The power output is proportional to the power dissipated in  $R_t$ , as expressed as

$$P_{out} = \frac{V_{out}^2}{R_t} \quad \text{where } V_{out} = \frac{R_t}{R_0 + R_t} V_{in} \quad (65.18)$$

The power available from the transmitter is

$$P_{in} = \frac{\left(V_{in}/2\right)^2}{R_0} \quad (65.19)$$

into a matched load. From the two previous equations, the power efficiency is

$$\frac{P_{out}}{P_{in}} = \frac{4R_0 R_t}{\left(R_0 + R_t\right)^2} \quad (65.20)$$

For a fixed-source impedance, the maximum efficiency is obtained by taking the derivative of Eq. (65.20) with respect to  $R_t$  and setting it to zero. Maximum efficiency occurs when the source impedance is matched to the transducer impedance,  $R_0 = R_t$ .

In practice, the transducer has a complex impedance of  $R_m$  in parallel with  $C_0$  (see Fig. 65.6), which is excited by a transmitter with a real impedance of  $50 \, \Omega$ . The transducer has a maximum efficiency

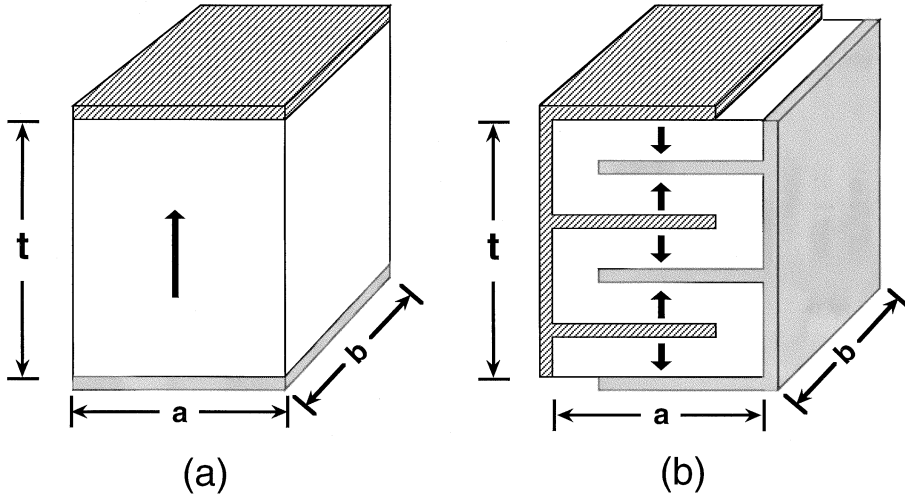


**FIGURE 65.9** (a) Conventional single-layer ceramic; (b) five-layer ceramic of the same overall dimensions. The layers are electrically in parallel and acoustically in series. The arrows indicate the piezoelectric poling directions of each layer.

when the imaginary component is tuned out and the real component is  $50 \Omega$ . This can be accomplished with electrical matching networks.

The capacitance  $C_0$  is tuned out in the frequency range near  $\omega_0$  using an inductor of

$$L_0 = \frac{1}{\omega_0^2 C_0} \quad (65.21)$$

for an inductor in shunt, or

$$L_1 = \frac{1}{\omega_0^2 C_0 + 1/R_m^2 C_0} \quad (65.22)$$

for an inductor in series. The example array elements described in the preceding subsection have  $C_0 = 22 \text{ pF}$  and  $R_m = 340 \Omega$  at series resonance of 5.0 MHz. Therefore, tuning inductors of  $L_0 = 46 \mu\text{H}$  or  $L_1 = 2.4 \mu\text{H}$  should be used.

A shunt inductor also raises the impedance of the transducer, as seen from the scanner, while a series inductor lowers the terminal impedance [Hunt et al., 1983]. For more significant changes in terminal impedance, transformers are used.

A transformer of turns ratio  $1:N$  multiplies the terminal impedance by  $1/N^2$ . In the transmit mode,  $N$  can be adjusted so that the terminal impedance matches the transmitter impedance. In the receive mode, the open-circuit sensitivity varies as  $1/N$  because of the step-down transformer. The lower terminal impedance of the array element, however, provides increased ability to drive an electrical load.

More complicated circuits can be used for better electrical matching across a wide bandwidth [Hunt et al., 1983]. These circuits can be either passive, as above, or active. Inductors also can be used in the scanner to tune out the capacitance of the coaxial cable that loads the transducer on receive.

Another alternative for electrical matching is to use multilayer piezoelectric ceramics [Goldberg and Smith, 1994]. Figure 65.9 shows an example of a single layer and a five-layer array element with the same overall dimensions of  $a$ ,  $b$ , and  $t$ . Since the layers are connected electrically in parallel, the clamped capacitance of a multilayer ceramic (MLC) element is

$$C_0 = N \cdot \epsilon^s \cdot \frac{ab}{t/N} = N^2 \cdot C_{\text{single}} \quad (65.23)$$

where  $C_{\text{single}}$  is the capacitance of the single-layer element (Eq. 65.8). As a result, the MLC impedance is reduced by a factor of  $N^2$ . Acoustically, the layers of the MLC are in series so the  $\lambda/2$  resonant thickness is  $t$ , the stack thickness.

To a first order, an  $N$ -layer ceramic has identical performance compared with a  $1:N$  transformer, but the impedance is transformed within the ceramic. MLCs also can be fabricated in large quantities more easily than hand-wound transformers. While MLCs do not tune out the reactive impedance, they make it easier to tune a low capacitance array element. By lowering the terminal impedance of an array element, MLCs significantly improve transducer SNR.

## Summary

The piezoelectric transducer is an important component in the ultrasound imaging system. The transducer often consists of a liner array that can electronically focus an acoustic beam. Depending on the configuration of array elements, the region scanned may be sector shaped or rectangular in two dimensions or pyramidal shaped in three dimensions.

The transducer performance large determines the resolution and the signal-to-noise ratio of the resulting ultrasound image. The design of an array involves many compromises in choosing operating frequency and array-element dimensions. Electrical matching networks and quarter-wave matching layers may be added to improve transducer performance.

Further improvements in transducer performance may result from several areas of research. Newer materials, such as composites, are gaining widespread use in medical ultrasound. In addition, 1.5D arrays or 2D arrays may be employed to control the acoustic beam in both azimuth and elevation. Problems in fabrication and electrical impedance matching must be overcome to implement these arrays in an ultrasound system.

## Defining Terms

**Acoustic impedance:** In an analogy to transmission line impedance, the acoustic impedance is the ratio of pressure to particle velocity in a medium; more commonly, it is defined as  $Z = \rho c$ , where  $\rho$  = density and  $c$  = speed of sound in a medium [the units are  $\text{kg}/(\text{m}^2 \cdot \text{sec})$  or Rayls].

**Angular response:** The radiation pattern versus angle for a single element of an array.

**Axial resolution:** The ability to distinguish between targets aligned in the axial direction (the direction of acoustic propagation).

**Azimuth dimension:** The lateral dimension that is along the scanning plane for an array transducer.

**Electrical matching networks:** Active or passive networks designed to tune out reactive components of the transducer and/or match the transducer impedance to the source and receiver impedance.

**Elevation dimension:** The lateral dimension that is perpendicular to the scanning plane for an array transducer.

**Grating lobes:** Undesirable artifacts in the radiation pattern of a transducer; they are produced at a location where the path length difference to adjacent array elements is a multiple of a wavelength.

**Lateral modes:** Transducer vibrations that occur in the lateral dimensions when the transducer is excited in the thickness dimension.

**Lateral resolution:** The ability to distinguish between targets in the azimuth and elevation dimensions (perpendicular to the axial dimension).

**Quarter-wave matching layers:** One or more layers of material placed between the transducer and the load medium (water or human tissue); they effectively match the acoustic impedance of the transducer to the load medium to improve the transducer bandwidth and signal-to-noise ratio.



## References

- Allen JL. 1964. Array antennas: New applications for an old technique. *IEEE Spect* 1:115.
- Berlincourt D. 1971. Piezoelectric crystals and ceramics. In OE Mattiat (ed), *Ultrasonic Transducer Materials*. New York, Plenum Press.
- Bobber RJ. 1970. Underwater Electroacoustic Measurements. Washington, Naval Research Laboratory.
- Christensen DA. 1988. *Ultrasonic Bioinstrumentation*. New York, Wiley.
- Curie P, Curie J. 1980. Development par pression de l'électricité polaire dans les cristaux hémiedres à faces enclinales. *Comp Rend* 91:383.
- Desilets CS, Fraser JD, Kino GS. 1978. The design of efficient broad-band piezoelectric transducers. *IEEE Trans Son Ultrason* SU-25:115.
- Flax SW, O'Donnell M. 1988. Phase aberration correction using signals from point reflectors and diffuse scatters: Basic principles. *IEEE Trans Ultrason Ferroelec Freq Contr* 35:758.
- Goldberg RL, Smith SW. 1994. Multi-layer piezoelectric ceramics for two-dimensional array transducers. *IEEE Trans Ultrason Ferroelec Freq Contr*.
- Goodman W. 1986. *Introduction to Fourier Optics*. New York, McGraw-Hill.
- Hunt JW, Arditi M, Foster FS. 1983. Ultrasound transducers for pulse-echo medical imaging. *IEEE Trans Biomed Eng* 30:453.
- Kino GS. 1987. *Acoustic Waves*. Englewood Cliffs, NJ, Prentice-Hall.
- Kino GS, Desilets CS. 1979. Design of slotted transducer arrays with matched backings. *Ultrason Imag* 1:189.
- Nock LF, Trahey GE. 1992. Synthetic receive aperture imaging with phase correction for motion and for tissue inhomogeneities: I. Basic principles. *IEEE Trans Ultrason Ferroelec Freq Contr* 39:489.
- Selfridge AR, Kino GS, Khuri-Yahub BT. 1980. A theory for the radiation pattern of a narrow strip acoustic transducer. *Appl Phys Lett* 37:35.
- Shattuck DP, Weinshenker MD, Smith SW, von Ramm OT. 1984. Explososcan: A parallel processing technique for high speed ultrasound imaging with linear phased arrays. *J Acoust Soc Am* 75:1273.
- Sherar MD, Foster FS. 1989. The design and fabrication of high frequency poly(vinylidene fluoride) transducers. *Ultrason Imag* 11:75.
- Smith WA. 1992. New opportunities in ultrasonic transducers emerging from innovations in piezoelectric materials. In FL Lizzi (ed), *New Developments in Ultrasonic Transducers and Transducer Systems*, 3–26. New York, SPIE.
- Somer JC. 1968. Electronic sector scanning for ultrasonic diagnosis. *Ultrasonics* 153.
- Steinberg BD. 1976. *Principles of Aperture and Array System Design*. New York, Wiley.
- Takeuchi H, Masuzawa H, Nakaya C, Ito Y. 1990. Relaxor ferroelectric transducers. *Proc IEEE Ultrasonics Symposium*, IEEE cat no 90CH2938-9, pp 697–705.
- Trahey GE, Zhao D, Miglin JA, Smith SW. 1990. Experimental results with a real-time adaptive ultrasonic imaging system for viewing through distorting media. *IEEE Trans Ultrason Ferroelec Freq Contr* 37:418.
- von Ramm OT, Smith SW. 1990. Real time volumetric ultrasound imaging system. In *SPIE Medical Imaging IV: Image Formation*, vol 1231, pp 15–22. New York, SPIE.
- von Ramm OT, Thurstone FL. 1976. Cardiac imaging using a phased array ultrasound system: I. System design. *Circulation* 53:258.

## Further Information

A good overview of linear array design and performance is contained in von O.T. Ramm and S.W. Smith (1983), Beam steering with linear arrays, *IEEE Trans Biomed Eng* 30:438. The same issue contains a more general article on transducer design and performance: J.W. Hunt, M. Arditi, and F.S. Foster (1983), Ultrasound transducers for pulse-echo medical imaging, *IEEE Trans Biomed Eng* 30:453.

The journal *IEEE Transactions on Ultrasonics, Ferroelectrics, and Frequency Control* frequently contains articles on medical ultrasound transducers. For subscription information, contact IEEE Service Center, 445 Hoes Lane, P.O. Box 1331, Piscataway, NJ 08855-1331, phone (800) 678-IEEE.

Another good source is the proceedings of the IEEE Ultrasonics Symposium, published each year. Also, the proceedings from *New Developments in Ultrasonics Transducers and Transducer Systems*, edited by F.L. Lizzi, was published by SPIE, Vol. 1733, in 1992.

## 65.2 Ultrasonic Imaging

---

*Jack G. Mottley*

It was recognized long ago that the tissues of the body are inhomogeneous and that signals sent into them, like pulses of high-frequency sound, are reflected and scattered by those tissues. Scattering, or redirection of some of an incident energy signal to other directions by small particles, is why we see the beam of a spotlight in fog or smoke. That part of the scattered energy that returns to the transmitter is called the backscatter.

Ultrasonic imaging of the soft tissues of the body really began in the early 1970s. At that time, the technologies began to become available to capture and display the echoes backscattered by structures within the body as images, at first as static compound images and later as real-time moving images. The development followed much the same sequence (and borrowed much of the terminology) as did radar and sonar, from initial crude single-line-of-sight displays (A-mode) to recording these side by side to build up recordings over time to show motion (M-mode), to finally sweeping the transducer either mechanically or electronically over many directions and building up two-dimensional views (B-mode or 2D).

Since this technology was intended for civilian use, applications had to wait for the development of inexpensive data handling, storage, and display technologies. A-mode was usually shown on oscilloscopes, M-modes were printed onto specially treated light-sensitive thermal paper, and B-mode was initially built up as a static image in analog scan converters and shown on television monitors. Now all modes are produced in real time in proprietary scan converters, shown on television monitors, and recorded either on commercially available videotape recorders (for organs or studies in which motion is a part of the diagnostic information) or as still frames on photographic film (for those cases in which organ dimensions and appearance are useful, but motion is not important).

Using commercial videotape reduces expenses and greatly simplifies the review of cases for quality control and training, since review stations can be set up in offices or conference rooms with commonly available monitors and videocassette recorders, and tapes from any imaging system can be played back. Also, the tapes are immediately available and do not have to be chemically processed.

Since the earliest systems were mostly capable of showing motion, the first applications were in studying the heart, which must move to carry out its function. A-mode and M-mode displays (see [Figs. 65.10](#) through [65.12](#)) were able to demonstrate the motion of valves, thickening of heart chamber walls, relationships between heart motion and pressure, and other parameters that enabled diagnoses of heart problems that had been difficult or impossible before. For some valvular diseases, the preferred display format for diagnosis is still the M-mode, on which the speed of valve motions can be measured and the relations of valve motions to the electrocardiogram (ECG) are easily seen.

Later, as 2D displays became available, ultrasound was applied more and more to imaging of the soft abdominal organs and in obstetrics ([Fig. 65.13](#)). In this format, organ dimensions and structural relations are seen more easily, and since the images are now made in real time, motions of organs such as the heart are still well appreciated. These images are used in a wide variety of areas from obstetrics and gynecology to ophthalmology to measure the dimensions of organs or tissue masses and have been widely accepted as a safe and convenient imaging modality.

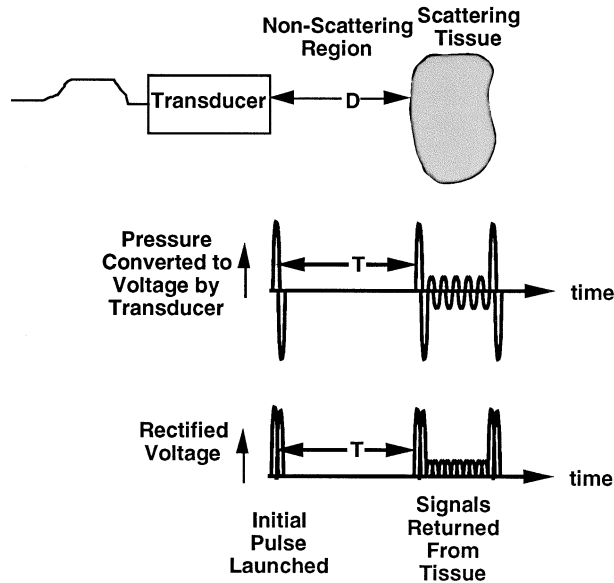


**FIGURE 65.10** Schematic representation of the signal received from along a single line of sight in a tissue. The rectified voltage signals are displayed for A-mode.

## Fundamentals

Strictly speaking, ultrasound is simply any sound wave whose frequency is above the limit of human hearing, which is usually taken to be 20 kHz. In the context of imaging of the human body, since frequency and wavelength (and therefore resolution) are inversely related, the lowest frequency of sound commonly used is around 1 MHz, with a constant trend toward higher frequencies in order to obtain better resolution. Axial resolution is approximately one wavelength, and at 1 MHz, the wavelength is 1.5 mm in most soft tissues, so one must go to 1.5 MHz to achieve 1-mm resolution.

Attenuation of ultrasonic signals increases with frequency in soft tissues, and so a tradeoff must be made between the depth of penetration that must be achieved for a particular application and the highest frequency that can be used. Applications that require deep penetration (e.g., cardiology, abdominal, obstetrics) typically use frequencies in the 2- to 5-MHz range, while those applications which only require shallow penetration but high resolution (e.g., ophthalmology, peripheral vascular, testicular) use frequencies up to around 20 MHz. Intra-arterial imaging systems, requiring submillimeter resolution, use even higher frequencies of 20 to 50 MHz, and laboratory applications of ultrasonic microscopy use frequencies up to 100 or even 200 MHz to examine structures within individual cells.

There are two basic equations used in ultrasonic imaging. One relates the (one-way) distance  $d$  of an object that caused an echo from the transducer to the (round-trip) time delay  $t$  and speed of sound in the medium  $c$ :

$$d = \frac{1}{2} tc \quad (65.24)$$

The speed of sound in soft body tissues lies in a fairly narrow range from 1450 to 1520 m/s. For rough estimates of time of flight, one often uses 1500 m/s, which can be converted to 1.5 mm/ $\mu$ s, a more convenient set of units. This leads to delay times for the longest-range measurements (20 cm) of 270  $\mu$ s. To allow echoes and reverberations to die out, one needs to wait several of these periods before launching the next interrogating pulse, so pulse repetition frequencies of about a kilohertz are possible.

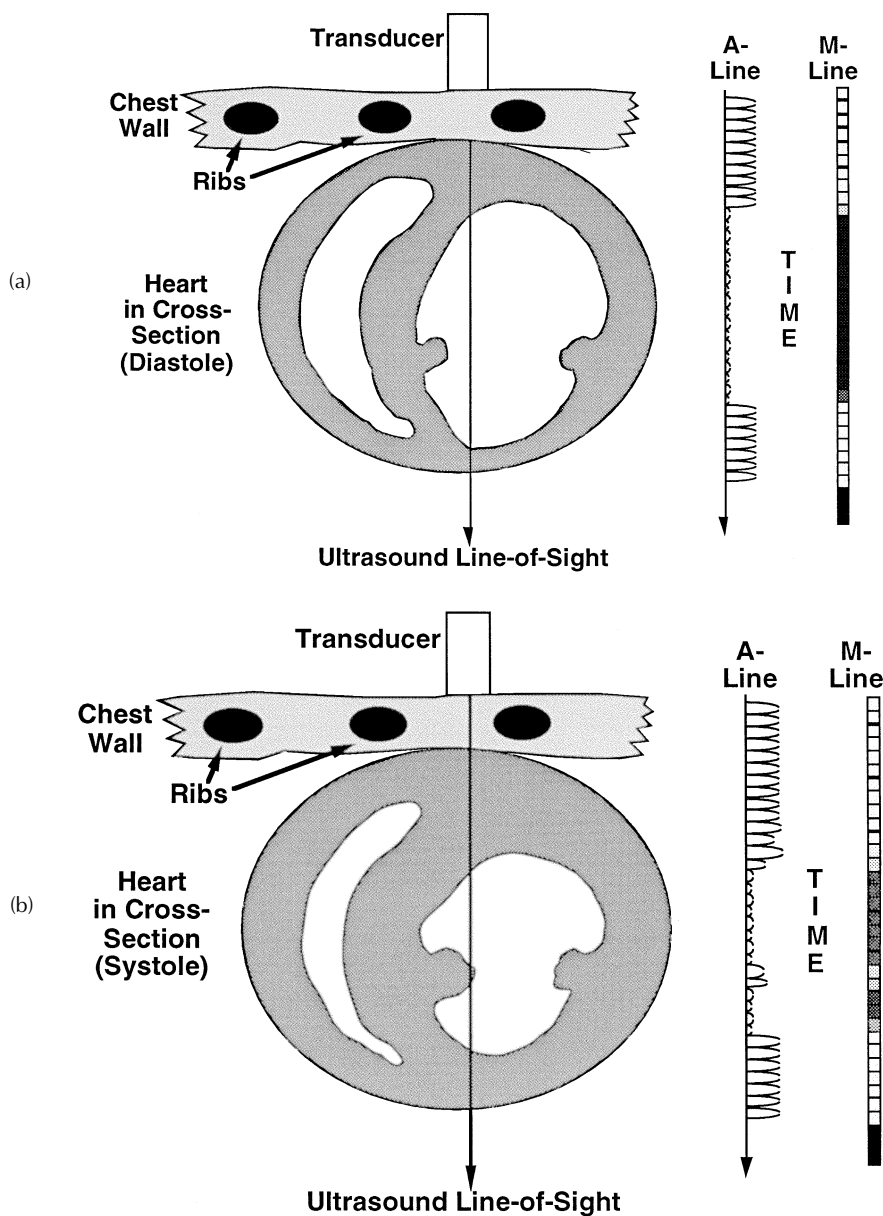


**FIGURE 65.11** Example of M-mode imaging of a heart at two points during the cardiac cycle. (a) Upper panel shows heart during diastole (relaxation) with a line of sight through it and the corresponding A-line converted to an M-line. (b) The lower panel shows the same heart during systole (contraction) and the A- and M-lines. Note the thicker walls and smaller ventricular cross-section during systole.

The other equation relates the received signal strength  $S(t)$  to the transmitted signal  $T(t)$ , the transducer's properties  $B(t)$ , the attenuation of the signal path to and from the scatterer  $A(t)$ , and the strength of the scatterer  $\eta(t)$ :

$$S(t) = T(t) \otimes B(t) \otimes A(t) \otimes \eta(t) \quad (65.25)$$

where  $\otimes$  denotes time-domain convolution. Using the property of Fourier transforms that a convolution in the time domain is a multiplication in the frequency domain, this is more often written in the frequency domain as

# M-Mode Echocardiogram

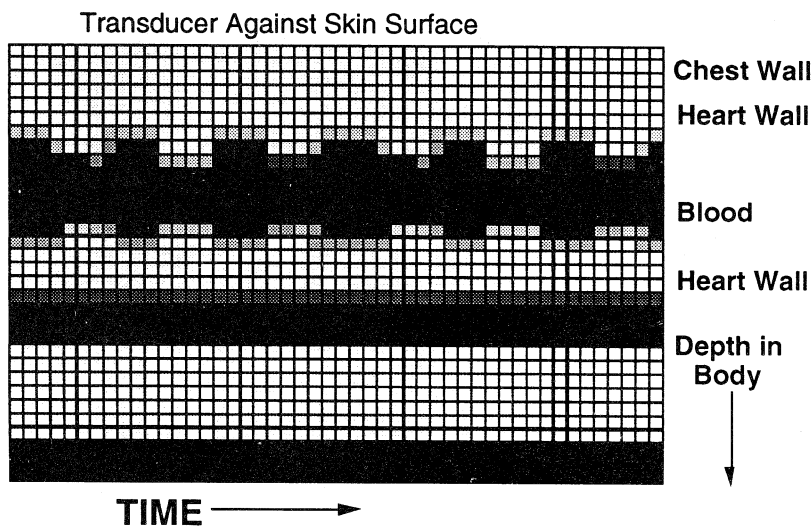


**FIGURE 65.12** Completed M-mode display obtained by showing the M-lines of Fig. 65.11 side by side. The motion of the heart walls and their thickening and thinning are well appreciated. Often the ECG or heart sounds are also shown in order to coordinate the motions of the heart with other physiologic markers.

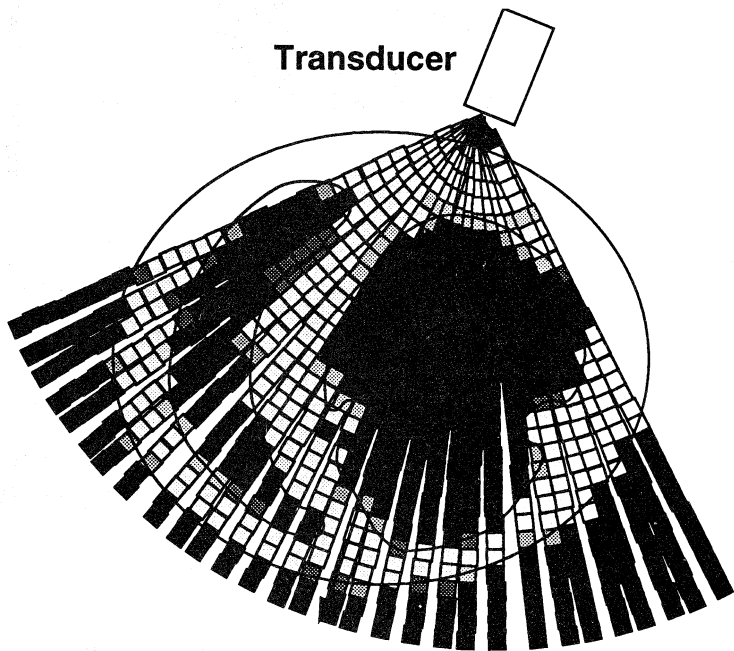


**FIGURE 65.13** Schematic representation of a heart and how a 2D image is constructed by scanning the transducer.

$$S(f) = T(f)B(f)A(f)\eta(f) \quad (65.26)$$

where each term is the Fourier transform of the corresponding term in the time-domain expression (65.25) and is written as a function of frequency  $f$ .

The goal of most imaging applications is to measure and produce an image based on the local values of the scattering strength, which requires some assumptions to be made concerning each of the other terms. The amplitude of the transmitted signal  $T(f)$  is a user-adjustable parameter that simply adds a scale factor to the image values, unless it increases the returned signal to the point of saturating the receiver amplifier. Increasing the transmit power increases the strength of return from distant or faint echoes simply by increasing the power that illuminates them, like using a more powerful flashlight lets you see farther at night. Some care must be taken to not turn the transmit power up too high, since very high power levels are capable of causing acoustic cavitation or local heating of tissues, both of which can cause cellular damage. Advances in both electronics and transducers make it possible to transmit more and more power. For this reason, new ultrasonic imaging systems are required to display an index value that indicates the transmitted power. If the index exceeds established thresholds, it is possible that damage may occur, and the examiner should limit the time of exposure.

Most imaging systems are fairly narrow band, so the transducer properties  $B(f)$  are constant and produce only a scale factor to the image values. On phased-array systems it is possible to change the depth of focus on both transmit and receive. This improves image quality and detection of lesions by matching the focusing characteristics of the transducer to best image the object in question, like focusing a pair of binoculars on a particular object.

As the ultrasonic energy travels along the path from transmitter to scatterer and back, attenuation causes the signal to decrease with distance. This builds up as a line integral from time 0 to time  $t$  as

$$A(f, t) = e^{-\int_0^t \alpha(f) c dt'}$$

An average value of attenuation can be corrected for electronically by increasing the gain of the imaging system as a function of time [variously called time gain compensation (TGC) or depth gain compensation (DGC)]. In addition, some systems allow for lateral portions of the image region to have different attenuation by adding a lateral gain compensation in which the gain is increased to either side of the center region of the image.

Time gain compensation is usually set to give a uniform gray level to the scattering along the center of the image. Most operators develop a “usual” setting on each machine, and if it becomes necessary to change those settings to obtain acceptable images on a patient, then that indicates that the patient has a higher attenuation or that there is a problem with the electronics, transducer, or acoustic coupling.

## Applications and Example Calculations

As an example of calculating the time of flight of an ultrasonic image, consider the following.

**Example 1.** A tissue has a speed of sound  $c = 1460$  m/s, and a given feature is 10 cm deep within. Calculate the time it will take an ultrasonic signal to travel from the surface to the feature and back.

**Answer:**  $t = 2 \times (10 \text{ cm}) / (1460 \text{ m/s}) = 137 \text{ } \mu\text{s}$ , where the factor of 2 is to account for the round trip the signal has to make (i.e., go in and back out).

**Example 2.** Typical soft tissues attenuate ultrasonic signals at a rate of 0.5 dB/cm/MHz. How much attenuation would be suffered by a 3-MHz signal going through 5 cm of tissue and returning?

**Answer:**  $a = 3 \text{ MHz} \times (0.5 \text{ dB/cm/MHz}) / (8.686 \text{ dB/neper}) = 0.173 \text{ neper/cm}$ ,  $A(3 \text{ MHz}, 5 \text{ cm}) = e^{(-0.173 \text{ neper/cm}) \times (5 \text{ cm}) \times 2} = 0.177$ .

## Economics

Ultrasonic imaging has many economic advantages over other imaging modalities. The imaging systems are typically much less expensive than those used for other modalities and do not require special preparations of facilities such as shielding for x-rays or uniformity of magnetic field for MRI. Most ultrasonic imaging systems can be rolled easily from one location to another, so one system can be shared among technicians or examining rooms or even taken to patients' rooms for critically ill patients.

There are minimal expendables used in ultrasonic examinations, mostly the coupling gel used to couple the transducer to the skin and videotape or film for recording. Transducers are reusable and amortized over many examinations. These low costs make ultrasonic imaging one of the least expensive modalities, far preferred over others when indicated. The low cost also means these systems can be a part of private practices and used only occasionally.

As an indication of the interest in ultrasonic imaging as an alternative to other modalities, in 1993, the *Wall Street Journal* reported that spending in the United States on MRI units was approximately \$520 million, on CT units \$800 million, and on ultrasonic imaging systems \$1000 million, and that sales of ultrasound systems was growing at 15% annually [1].

## Defining Terms

**A-mode:** The original display of ultrasound measurements, in which the amplitude of the returned echoes along a single line is displayed on an oscilloscope.

**Attenuation:** The reduction in signal amplitude that occurs per unit distance traveled. Some attenuation occurs in homogeneous media such as water due to viscous heating and other phenomena, but that is very small and is usually taken to be negligible over the 10- to 20-cm distances typical of imaging systems. In inhomogeneous media such as soft tissues, the attenuation is much higher and increases with frequency. The values reported for most soft tissues lie around 0.5 dB/cm/MHz.

**Backscatter:** That part of a scattered signal that goes back toward the transmitter of the energy.

**B-mode or 2D:** The current display mode of choice. This is produced by sweeping the transducer from side to side and displaying the strength of the returned echoes as bright spots in their geometrically correct direction and distance.

**Compound images:** Images built up by adding, or compounding, data obtained from a single transducer or multiple transducers swept through arcs. Often these transducers were not fixed to a single point of rotation but could be swept over a surface of the body like the abdomen in order to build up a picture of the underlying organs such as the liver. This required an elaborate position-sensing apparatus attached to the patient's bed or the scanner and that the organ in question be held very still throughout the scanning process, or else the image was blurred.

**M-mode:** Followed A-mode by recording the strength of the echoes as dark spots on moving light-sensitive paper. Objects that move, such as the heart, caused standard patterns of motion to be displayed, and a lot of diagnostic information such as valve closure rates, whether valves opened or closed completely, and wall thickness could be obtained from M-mode recordings.

**Real-time images:** Images currently made on ultrasound imaging systems by rapidly sweeping the transducer through an arc either mechanically or electronically. Typical images might have 120 scan lines in each image, each 20 cm long. Since each line has a time of flight of 267  $\mu$ s, a single frame takes  $120 \times 267 \mu\text{s} = 32 \text{ ms}$ . It is therefore possible to produce images at standard video frame rates (30 frames/sec, or 33.3 msec/frame).

**Reflection:** Occurs at interfaces between large regions (much larger than a wavelength) of media with differing acoustic properties such as density or compressibility. This is similar to the reflection of light at interfaces and can be either *total*, like a mirror, or *partial*, like a half-silvered mirror or the ghostlike reflection seen in a sheet of glass.

**Scattering:** Occurs when there are irregularities or inhomogeneities in the acoustic properties of a medium over distances comparable with or smaller than the wavelength of the sound. Scattering from objects much smaller than a wavelength typically increases with frequency (the blue-sky law in optics), while that from an object comparable to a wavelength is constant with frequency (why clouds appear white).

## Reference

1. Naj AK. 1993. Industry focus: Big medical equipment makers try ultrasound market; cost-cutting pressures prompt shift away from more expensive devices. *Wall Street Journal*, November 30, B-4.

## Further Information

There are many textbooks that contain good introduction to ultrasonic imaging. *Physical Principles of Ultrasonic Diagnosis*, by P. N. Wells, is a classic, and there is a new edition of another classic, *Diagnostic Ultrasound: Principles, Instruments and Exercises*, 4th ed., by Frederick Kremkau. Books on medical imaging that contain introductions to ultrasonic imaging include *Medical Imaging Systems*, by Albert Macovski; *Principles of Medical Imaging*, by Kirk Shung, Michael Smith, and Benjamin Tsui; and *Foundations of Medical Imaging*, by Zang-Hee Cho, Joie P. Jones, and Manbir Singh.

The monthly journals *IEEE Transactions on Ultrasonics, Ferroelectrics, and Frequency Control* and *IEEE Transactions on Biomedical Engineering* often contain information and research reports on ultrasonic imaging. For subscription information, contact IEEE Service Center, 445 Hoes Lane, P.O. Box 1331, Piscataway, NJ 08855-1331, phone (800) 678-4333. Another journal that often contains articles on ultrasonic imaging is the *Journal of the Acoustical Society of America*. For subscription information, contact AIP Circulation and Fulfillment Division, 500 Sunnyside Blvd., Woodbury, NY 11797-2999, phone (800) 344-6908; e-mail: [elecprod@pinet.aip.org](mailto:elecprod@pinet.aip.org).

There are many journals that deal with medical ultrasonic imaging exclusively. These include *Ultrasonic Imaging*, the *Journal of Ultrasound in Medicine*, American Institute of Ultrasound of Medicine (AIUM), 14750 Sweitzer Lane, Suite 100, Laurel, MD 20707-5906, and the *Journal of Ultrasound in Medicine and Biology*, Elsevier Science, Inc., 660 White Plains Road, Tarrytown, NY 10591-5153, e-mail: [esuk.usa@elsevier.com](mailto:esuk.usa@elsevier.com).

There are also specialty journals for particular medical areas, e.g., the *Journal of the American Society of Echocardiography*, that are available through medical libraries and are indexed in Index Medicus, Current Contents, Science Citation Index, and other databases.

## 65.3 Blood Flow Measurement Using Ultrasound

---

### *K. Whittaker Ferrara*

In order to introduce the fundamental challenges of blood velocity estimation, a brief description of the unique operating environment produced by the ultrasonic system, intervening tissue, and the scattering of ultrasound by blood is provided. In providing an overview of the parameters that differentiate this problem from radar and sonar target estimation problems, an introduction to the fluid dynamics of the cardiovascular system is presented, and the requirements of specific clinical applications are summarized. An overview of blood flow estimation systems and their performance limitations is then presented. Next, an overview of the theory of moving target estimation, with its roots in radar and sonar signal processing, is provided. The application of this theory to blood velocity estimation is then reviewed, and a number of signal processing strategies that have been applied to this problem are considered. Areas of new research including three-dimensional (3D) velocity estimation and the use of ultrasonic contrast agents are described in the final section.

## Fundamental Concepts

In blood velocity estimation, the goal is not simply to estimate the mean target position and mean target velocity. The goal instead is to measure the velocity profile over the smallest region possible and to repeat this measurement quickly and accurately over the entire target. Therefore, the joint optimization of spatial, velocity, and temporal resolution is critical. In addition to the mean velocity, diagnostically useful information is contained in the volume of blood flowing through various vessels, spatial variations in



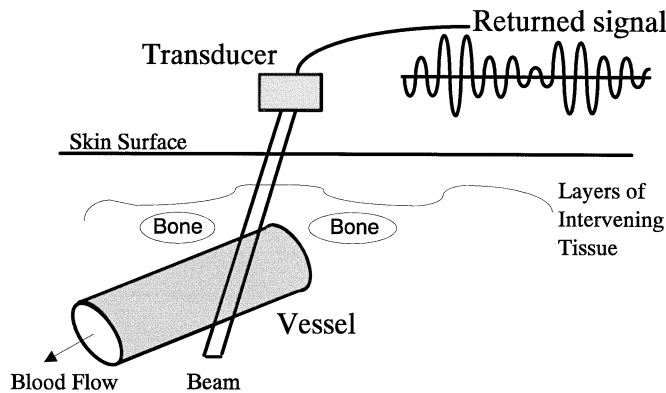


**FIGURE 65.14** Operating environment for the estimation of blood velocity.

the velocity profile, and the presence of turbulence. While current methods have proven extremely valuable in the assessment of the velocity profile over an entire vessel, improved *spatial resolution* is required in several diagnostic situations. Improved *velocity resolution* is also desirable for a number of clinical applications. Blood velocity estimation algorithms implemented in current systems also suffer from a velocity ambiguity due to aliasing.

### Unique Features of the Operating Environment

A number of features make blood flow estimation distinct from typical radar and sonar target estimation situations. The combination of factors associated with the beam formation system, properties of the intervening medium, and properties of the target medium lead to a difficult and unique operating environment. [Figure 65.14](#) summarizes the operating environment of an ultrasonic blood velocity estimation system, and [Table 65.2](#) summarizes the key parameters.

**Beam Formation–Data Acquisition System.** *The transducer bandwidth is limited.* Most current transducers are limited to a 50% to 75% fractional bandwidth due to their finite dimensions and a variety of electrical and mechanical properties. This limits the form of the transmitted signal. The transmitted pulse is typically a short pulse with a carrier frequency, which is the center frequency in the spectrum of the transmitted signal.

*Federal agencies monitor four distinct intensity levels.* The levels are *TASA*, *TASP*, *TPSA*, and *TPSP*, where *T* represents temporal, *S* represents spatial, *A* represents average, and *P* represents peak. Therefore, the

**TABLE 65.2** Important Parameters

|  |  |
|--|--|
| Typical transducer center frequency            | 2–10 MHz   |
| Maximum transducer fractional bandwidth        | 50–75%   |
| Speed of sound $c$                             | 1500–1600 m/s                                    |
| Acoustic wavelength ( $c = 1540$ )             | 0.154–1.54 mm                                    |
| Phased-array size                              | $>32 \cdot \text{wavelength}$                    |
| Sample volume size                             | $\text{mm}^3$                                    |
| Blood velocity                                 | Normal; up to 1 m/s<br>Pathological: up to 8 m/s |
| Vessel wall echo/blood echo                    | 20–40 dB   |
| Diameter of a red blood cell                   | 8.5 $\mu\text{m}$                                |
| Thickness of a red blood cell                  | 2.4 $\mu\text{m}$                                |
| Volume of a red blood cell                     | $87 \pm 6 \mu\text{m}^3$                         |
| Volume concentration of cells (hematocrit)     | 45%  |
| Maximum concentration without cell deformation | 58%  |

use of long bursts requires a proportionate reduction in the transmitted peak power. This may limit the signal-to-noise ratio (SNR) obtained with a long transmitted burst due to the weak reflections from the complex set of targets within the body.

**Intervening Medium.** Acoustic windows, which are locations for placement of a transducer to successfully interrogate particular organs, are limited in number and size. Due to the presence of bone and air, the number of usable acoustic windows is extremely limited. The reflection of acoustic energy from bone is only 3 dB below that of a perfect reflector [Wells, 1977]. Therefore, transducers cannot typically surround a desired imaging site. In many cases, it is difficult to find a single small access window. This limits the use of inverse techniques.

Intervening tissue produces acoustic refraction and reflection. Energy is reflected at unpredictable angles.

The clutter-to-signal ratio is very high. Clutter is the returned signal from stationary or slowly moving tissue, which can be 40 dB above the returned signal from blood. Movement of the vessel walls and valves during the cardiac cycle introduces a high-amplitude, low-frequency signal. This is typically considered to be unwanted noise, and a high-pass filter is used to eliminate the estimated wall frequencies.

The sampling rate is restricted. The speed of sound in tissue is low (approximately 1540 m/s), and each transmitted pulse must reach the target and return before the returned signal is recorded. Thus the sampling rate is restricted, and the aliasing limit is often exceeded.

The total observation time is limited (due to low acoustic velocity). In order to estimate the velocity of blood in all locations in a 2D field in real time, the estimate for each region must be based on the return from a limited number of pulses because of the low speed of sound.

Frequency-dependent attenuation affects the signal. Tissue acts as a low-pass transmission filter; the scattering functions as a high-pass filter. The received signal is therefore a distorted version of the transmitted signal. In order to estimate the effective filter function, the type and extent of each tissue type encountered by the wave must be known. Also, extension of the bandwidth of the transmitted signal to higher frequencies increases absorption, requiring higher power levels that can increase health concerns.

**Target Scattering Medium (Red Blood Cells).** Multiple groups of scatterers are present. The target medium consists of multiple volumes of diffuse moving scatterers with velocity vectors that vary in magnitude and direction. The target medium is spread in space and velocity. The goal is to estimate the velocity over the smallest region possible.

There is a limited period of statistical stationarity. The underlying cardiac process can only be considered to be stationary for a limited time. This time was estimated to be 10 ms for the arterial system by Hatle and Angelsen [1985]. If an observation interval greater than this period is used, the average scatterer velocity cannot be considered to be constant.

## Overview of Ultrasonic Flow Estimation Systems

Current ultrasonic imaging systems operate in a pulse-echo (PE) or continuous-wave (CW) intensity mapping mode. In pulse-echo mode, a very short pulse is transmitted, and the reflected signal is analyzed. For a continuous-wave system, a lower-intensity signal is continuously transmitted into the body, and the reflected energy is analyzed. In both types of systems, an acoustic wave is launched along a specific path into the body, and the return from this wave is processed as a function of time. The return is due to reflected waves from structures along the line of sight, combined with unwanted noise. Spatial selectivity is provided by beam formation performed on burst transmission and reception. Steering of the beam to a particular angle and creating a narrow beam width at the depth of interest are accomplished by an effective lens applied to the ultrasonic transducer. This lens may be produced by a contoured material, or it may be simulated by phased pulses applied to a transducer array. The spatial weighting pattern will ultimately be the product of the effective lens on transmission and reception. The returned signal from the formed beam can be used to map the backscattered intensity into a two-dimensional gray-scale image, or to estimate target velocity. *We shall focus on the use of this information to estimate the velocity of red blood cells moving through the body.*

**Single Sample Volume Doppler Instruments.** One type of system uses the Doppler effect to estimate velocity in a single volume of blood, known as the sample volume, which is designated by the system operator. The Doppler shift frequency from a moving target can be shown to equal  $2f_c v/c$ , where  $f_c$  is the transducer center frequency in Hertz,  $c$  is the speed of sound within tissue, and  $v$  is the velocity component of the blood cells toward or away from the transducer. These “Doppler” systems transmit a train of long pulses with a well-defined carrier frequency and measure the Doppler shift in the returned signal. The spectrum of Doppler frequencies is proportional to the distribution of velocities present in the sample volume. The sample volume is on a cubic millimeter scale for typical pulse-echo systems operating in the frequency range of 2 to 10 MHz. Therefore, a thorough cardiac or peripheral vascular examination requires a long period. In these systems, 64 to 128 temporal samples are acquired for each estimate. The spectrum of these samples is typically computed using a fast Fourier transform (FFT) technique [Kay and Marple, 1981]. The range of velocities present within the sample volume can then be estimated. The spectrum is scaled to represent velocity and plotted on the vertical axis. Subsequent spectral estimates are then calculated and plotted vertically adjacent to the first estimate.

**Color Flow Mapping.** In color flow mapping, a pseudo-color velocity display is overlaid on a 2D gray-scale image. Simultaneous amplitude and velocity information is thus available for a 2D sector area of the body. The clinical advantage is a reduction in the examination time and the ability to visualize the velocity profile as a 2D map. Figure 65.15 shows a typical color flow map of ovarian blood flow combined with the Doppler spectrum of the region indicated by the small graphic sample volume. The color flow map shows color-encoded velocities superimposed on the gray-scale image with the velocity magnitude indicated by the color bar on the side of the image. Motion toward the transducer is shown in yellow and red, and motion away from the transducer is shown in blue and green, with the range of colors representing a range of velocities to a maximum of 6 cm/s in each direction. Velocities above this limit would produce aliasing for the parameters used in optimizing the instrument for the display of ovarian flow. A velocity of 0 m/s would be indicated by black, as shown at the center of the color bar. Early discussions of the implementation of color flow mapping systems can be found in Curry and White [1978] and Nowicki and Reid [1981].

The lower portion of the image presents an intensity-modulated display of instantaneous Doppler components along the vertical axis. As time progresses, the display is translated along the horizontal axis to generate a Doppler time history for the selected region of interest [provided by Acuson Corporation, Mountain View, Calif.].

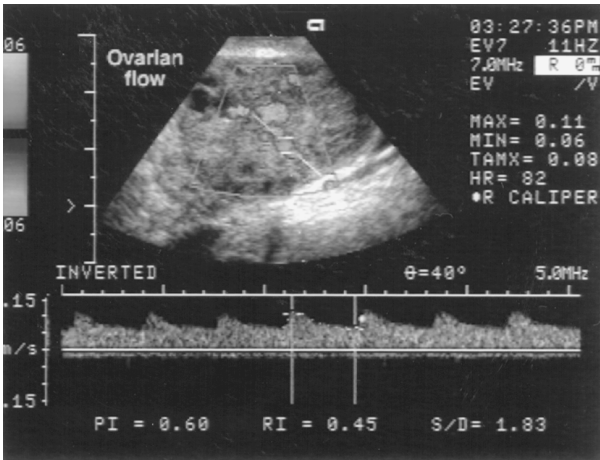


FIGURE 65.15 Flow map and Doppler spectrum for ovarian blood flow.

Limitations of color flow instruments result in part from the transmission of a narrowband (long) pulse that is needed for velocity estimation but degrades spatial resolution and prevents mapping of the spatial-velocity profile. Due to the velocity gradient in each blood vessel, the transmission of a long pulse also degrades the velocity resolution. This is caused by the simultaneous examination of blood cells moving at different velocities and the resulting mixing of regions of the scattering medium, which can be distinctly resolved on a conventional B-mode image. Since the limited speed of acoustic propagation velocity limits the sampling rate, a second problem is aliasing of the Doppler frequency. Third, information regarding the presence of velocity gradients and turbulence is desired and is not currently available. Finally, estimation of blood velocity based on the Doppler shift provides only an estimate of the axial velocity, which is the movement toward or away from the transducer, and cannot be used to estimate movement across the transducer beam. It is the 3D velocity magnitude that is of clinical interest.

For a color flow map, the velocity estimation technique is based on estimation of the mean Doppler shift using signal-processing techniques optimized for rapid (real-time) estimation of velocity in each region of the image. The transmitted pulse is typically a burst of 4 to 8 cycles of the carrier frequency. Data acquisition for use in velocity estimation is interleaved with the acquisition of information for the gray-scale image. Each frame of acquired data samples is used to generate one update of the image display. An azimuthal line is a line that describes the direction of the beam from the transducer to the target. A typical 2D ultrasound scanner uses 128 azimuthal lines per frame and 30 frames per second to generate a gray-scale image. Data acquisition for the velocity estimator used in color flow imaging requires an additional 4 to 18 transducer firings per azimuthal line and therefore reduces both the number of azimuthal lines and the number of frames per second. If the number of lines per frame is decreased, spatial undersampling or a reduced examination area results. If the number of frames per second is decreased, temporal undersampling results, and the display becomes difficult to interpret.

The number of data samples available for each color flow velocity estimate is reduced to 4 to 18 in comparison with the 64 to 128 data samples available to estimate velocity in a single sample volume Doppler mode. This reduction, required to estimate velocity over the 2D image, produces a large increase in the estimator variance.

## Fluid Dynamics and the Cardiovascular System

In order to predict and adequately assess blood flow profiles within the body, the fluid dynamics of the cardiovascular system will be briefly reviewed. The idealized case known as *Poiseuille flow* will be considered first, allowed by a summary of the factors that disturb Poiseuille flow.

A Poiseuille flow model is appropriate in a long rigid circular pipe at a large distance from the entrance. The velocity in this case is described by the equation  $v/v_0 = 1 - (r/a)^2$ , where  $v$  represents the velocity parallel to the wall,  $v_0$  represents the center-line velocity,  $r$  is the radial distance variable, and  $a$  is the radius of the tube. In this case, the mean velocity is half the center-line velocity, and the volume flow rate is given by the mean velocity multiplied by the cross-sectional area of the vessel.

For the actual conditions within the arterial system, Poiseuille flow is only an approximation. The actual arterial geometry is tortuous and individualistic, and the resulting flow is perturbed by entrance effects and reflections. Reflections are produced by vascular branches and the geometric taper of the arterial diameter. In addition, spatial variations in vessel elasticity influence the amplitude and wave velocity of the arterial pulse. Several parameters can be used to characterize the velocity profile, including the Reynolds number, the Womersley number, the pulsatility index, and the resistive index. The pulsatility and resistive indices are frequently estimated during a clinical examination.

The Reynolds number is denoted  $Re$  and measures the ratio of fluid inertia to the viscous forces acting on the fluid. The Reynolds number is defined by  $Re = Dv'/\mu_k$ , where  $v'$  is the average cross-sectional velocity,  $\mu_k$  is the kinematic viscosity, and  $D$  is the vessel diameter. *Kinematic viscosity* is defined as the fluid viscosity divided by the fluid density. When the Reynolds number is high, fluid inertia dominates. This is true in the aorta and larger arteries, and bursts of turbulence are possible. When the number is low, viscous effects dominate.

The Womersly number is used to describe the effect introduced by the unsteady, pulsatile nature of the flow. This parameter, defined by  $a(\omega/\mu_k)^{1/2}$ , where  $\omega$  represents radian frequency of the wave, governs propagation along an elastic, fluid-filled tube. When the Womersly number is small, the instantaneous profile will be parabolic in shape, the flow is viscous dominated, and the profile is oscillatory and Poiseuille in nature. When the Womersly number is large, the flow will be blunt, inviscid, and have thin wall layers [Nicholas and O'Rourke, 1990].

The pulsatility index represents the ratio of the unsteady and steady velocity components of the flow. This shows the magnitude of the velocity changes that occur during acceleration and deceleration of blood constituents. Since the arterial pulse decreases in magnitude as it travels, this index is maximum in the aorta. The pulsatility index is given by the difference between the peak systolic and minimum diastolic values divided by the average value over one cardiac cycle. The Pourcelot, or resistance, index is the peak-to-peak swing in velocity from systole to diastole divided by the peak systolic value [Nichols and O'Rourke, 1990].

**Blood Velocity Profiles.** Specific factors that influence the blood velocity profile include the entrance effect, vessel curvature, skewing, stenosis, acceleration, secondary flows, and turbulence. These effects are briefly introduced in this subsection.

The entrance effect is a result of fluid flow passing from a large tube or chamber into a smaller tube. The velocity distribution at the entrance becomes blunt. At a distance known as the *entry length*, the fully developed parabolic profile is restored, where the entry length is given by  $0.06\text{Re} \cdot (2a)$  [Nerem, 1985]. Distal to this point the profile is independent of distance.

If the vessel is curved, there will also be an entrance effect. The blunt profile in this case is skewed, with the peak velocity closer to the inner wall of curvature. When the fully developed profile occurs downstream, the distribution will again be skewed, with the maximal velocity toward the outer wall of curvature. Skewing also occurs at a bifurcation where proximal flow divides into daughter vessels. The higher-velocity components, which occurred at the center of the parent vessel, are then closer to the flow divider, and the velocity distribution in the daughter vessels is skewed toward the divider.

Stenosis, a localized narrowing of the vessel diameter, dampens the pulsatility of the flow and pressure waveforms. The downstream flow profile depends on the shape and degree of stenosis. Acceleration adds a flat component to the velocity profile. It is responsible for the flat profile during systole, as well as the negative flat component near the walls in the deceleration phase.

Secondary flows are swirling components which are superimposed on the main velocity profile. These occur at bends and branches, although regions of secondary flow can break away from the vessel wall and are then known as *separated flow*. These regions reattach to the wall at a point downstream.

One definition of turbulent flow is flow that demonstrates a random fluctuation in the magnitude and direction of velocity as a function of space and time. The intensity of turbulence is calculated using the magnitude of the fluctuating velocities. The relative intensity of turbulence is given by  $I_t = u_{\text{rms}}/u_{\text{mean}}$ , where  $u_{\text{rms}}$  represents the root-mean-square value of the fluctuating portion of the velocity, and  $u_{\text{mean}}$  represents the nonfluctuating mean velocity [Hinze, 1975].

## Clinical Applications and Their Requirements

Blood flow measurement with ultrasound is used in estimating the velocity and volume of flow within the heart and peripheral arteries and veins. Normal blood vessels vary in diameter up to a maximum of 2 cm, although most vessels examined with ultrasound have a diameter of 1 to 10 mm. Motion of the vessel wall results in a diameter change of 5% to 10% during a cardiac cycle.

**Carotid Arteries (Common, Internal, External).** The evaluation of flow in the carotid arteries is of great clinical interest due to their importance in supplying blood to the brain, their proximity to the skin, and the wealth of experience that has been developed in characterizing vascular pathology through an evaluation of flow. The size of the carotid arteries is moderate; they narrow quickly from a maximum diameter of 0.8 cm. The shape of carotid flow waveforms over the cardiac cycle can be related to the

pathophysiology of the circulation. Numerous attempts have been made to characterize the parameters of carotid waveforms and to compare these parameters in normal and stenotic cases. A number of indices have been used to summarize the information contained in these waveforms. The normal range of the Pourcelot index is 0.55 to 0.75. Many researchers have shown that accurate detection of a minor stenosis requires accurate quantitation of the entire Doppler spectrum and remains very difficult with current technology. The presence of a stenosis causes spectral broadening with the introduction of lower frequency or velocity components.

**Cardiology.** Blood velocity measurement in cardiology requires analysis of information at depths up to 18 cm. A relatively low center frequency (e.g., 2.5 to 3.5 MHz) typically is used in order to reduce attenuation. Areas commonly studied and the maximum rate of flow include the following [Hatle, 1985]:

| Normal Adult Maximal Velocity (m/s) |      |
|-------------------------------------|------|
| Mitral flow                         | 0.9  |
| Tricuspid flow                      | 0.5  |
| Pulmonary artery                    | 0.75 |
| Left ventricle                      | 0.9  |

**Aorta.** Aortic flow exhibits a blunt profile with entrance region characteristics. The entrance length is approximately 30 cm. The vessel diameter is approximately 2 cm. The mean Reynolds number is 2500 [Nerem, 1985], although the peak Reynolds number in the ascending aorta can range from 4300 to 8900, and the peak Reynolds number in the abdominal aorta is in the range of 400 to 1100 [Nichols and O'Rourke, 1990]. The maximal velocity is on the order of 1.35 m/s. The flow is skewed in the aortic arch with a higher velocity at the inner wall. The flow is unsteady and laminar with possible turbulent bursts at peak systole.

**Peripheral Arteries** [Hatsukami et al., 1992]. The peak systolic velocity in centimeters per second and standard deviation of the velocity measurement technique are provided below for selected arteries.

| Artery                  | Peak Systolic Velocity (cm/s) | Standard Deviation |
|-------------------------|-------------------------------|--------------------|
| Proximal external iliac | 99                            | 22                 |
| Distal external iliac   | 96                            | 13                 |
| Proximal common femoral | 89                            | 16                 |
| Distal common femoral   | 71                            | 15                 |
| Proximal popliteal      | 53                            | 9                  |
| Distal popliteal        | 53                            | 24                 |
| Proximal peroneal       | 46                            | 14                 |
| Distal peroneal         | 44                            | 12                 |

Nearly all the vessels above normally show some flow reversal during early diastole. A value of the pulsatility index of 5 or more in a limb artery is considered to be normal.

## Velocity Estimation Techniques

Prior to the basic overview of theoretical approaches to target velocity estimation, it is necessary to understand a few basic features of the received signal from blood scatterers. It is the statistical correlation of the received signal in space and time that provides the opportunity to use a variety of velocity estimation strategies. Velocity estimation based on analysis of the frequency shift or the temporal correlation can be justified by these statistical properties.

Blood velocity mapping has unique features due to the substantial viscosity of blood and the spatial limitations imposed by the vessel walls. Because of these properties, groups of red blood cells can be tracked over a significant distance. Blood consists of a viscous incompressible fluid containing an average

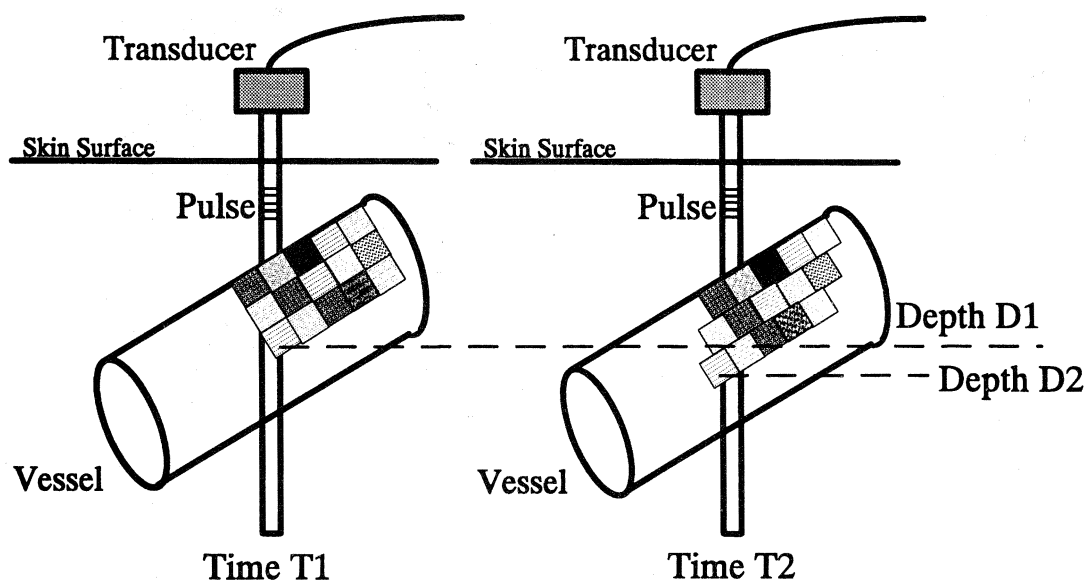


**FIGURE 65.16** Random concentration of red blood cells within a vessel at times  $T_1$  and  $T_2$ , where the change in depth from  $D_1$  to  $D_2$  would be used to estimate velocity.

volume concentration of red blood cells of 45%, although this concentration varies randomly through the blood medium. The red blood cells are primarily responsible for producing the scattered wave, due to the difference in their acoustic properties in comparison with plasma. Recent research into the characteristics of blood has led to stochastic models for its properties as a function of time and space [Angelson, 1980; Atkinson and Berry, 1974; Mo and Cobbold, 1986; Shung et al., 1976, 1992]. The scattered signal from an insonified spatial volume is a random process that varies with the fluctuations in the density of scatterers in the insonified area, the shear rate within the vessel, and the hematocrit [Atkinson and Berry, 1974; Ferrara and Algazi, 1994a, 1994b; Mo and Cobbold, 1986].

Since the concentration of cells varies randomly through the vessel, the magnitude of the returned signal varies when the group of scatterers being insonified changes. The returned amplitude from one spatial region is independent of the amplitude of the signal from adjacent spatial areas. As blood flows through a vessel, it transports cells whose backscattered signals can be tracked to estimate flow velocities.

Between the transmission of one pulse and the next, the scatterers move a small distance within the vessel. As shown in Fig. 65.16, a group of cells with a particular concentration which are originally located at depth  $D_1$  at time  $T_1$  move to depth  $D_2$  at time  $T_2$ . The resulting change in axial depth produces a change in the delay of the signal returning to the transducer from each group of scatterers. This change in delay of the radiofrequency (RF) signal can be estimated in several ways. As shown in Fig. 65.17, the returned signal from a set of sequential pulses then shows a random amplitude that can be used to estimate the velocity. Motion is detected using signal-processing techniques that estimate the shift of the signal between pulses.

**Clutter.** In addition to the desired signal from the blood scatterers, the received signal contains clutter echoes returned from the surrounding tissue. An important component of this clutter signal arises from slowly moving vessel walls. The wall motion produces Doppler frequency shifts typically below 1 kHz, while the desired information from the blood cells exists in frequencies up to 15 kHz. Due to the smooth structure of the walls, energy is scattered coherently, and the clutter signal can be 40 dB above the scattered signal from blood. High-pass filters have been developed to remove the unwanted signal from the surrounding vessel walls.

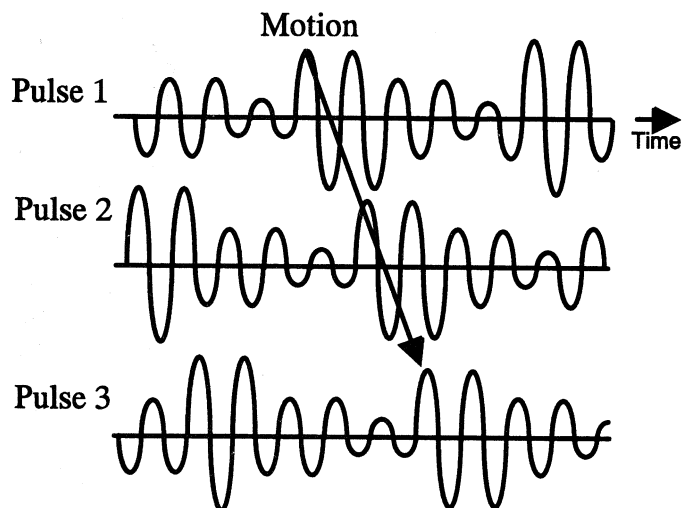


**FIGURE 65.17** Received RF signal from three transmitted pulses, with a random amplitude which can be used to estimate the axial movement of blood between pulses. Motion is shown by the shift in the signal with a recognizable amplitude.

**Classic Theory of Velocity Estimation.** Most current commercial ultrasound systems transmit a train of long pulses with a carrier frequency of 2 to 10 MHz and estimate velocity using the Doppler shift of the reflected signal. The transmission of a train of short pulses and new signal-processing strategies may improve the spatial resolution and quality of the resulting velocity estimate. In order to provide a basis for discussion and comparison of these techniques, the problem of blood velocity estimation is considered in this subsection from the view of classic velocity estimation theory typically applied to radar and sonar problems.

Important differences exist between classic detection and estimation for radar and sonar and the application of such techniques to medical ultrasound. The Van Trees [1971] approach is based on joint estimation of the Doppler shift and position over the entire target. In medical ultrasound, the velocity is estimated in small regions of a large target, where the target position is assumed to be known. While classic theories have been developed for estimation of all velocities within a large target by Van Trees and others, such techniques require a model for the velocity in each spatial region of interest. For the case of blood velocity estimation, the spatial variation in the velocity profile is complex, and it is difficult to postulate a model that can be used to derive a high-quality estimate. The theory of velocity estimation in the presence of spread targets is also discussed by Kennedy [1969] and Price [1968] as it applies to radar astronomy and dispersive communication channels.

It is the desire to improve the spatial and velocity resolution of the estimate of blood velocity that has motivated the evaluation of alternative wideband estimation techniques. Narrowband velocity estimation techniques use the Doppler frequency shift produced by the moving cells with a sample volume that is fixed in space. Wideband estimation techniques incorporate the change in delay of the returned pulse due to the motion of the moving cells. Within the classification of narrowband techniques are a number of estimation strategies to be detailed below. These include the fast Fourier transform (FFT), finite derivative estimation, the autocorrelator, and modern spectral estimation techniques, including autoregressive strategies. Within the classification of wideband techniques are cross-correlation strategies and the wideband maximum likelihood estimator (WMLE).

For improving the spatial mapping of blood velocity within the body, the transmission of short pulses is desirable. Therefore, it is of interest to assess the quality of velocity estimates made using narrowband and wideband estimators with transmitted signals of varying lengths. If  $(2v/c)BT \ll 1$ , where  $v$  represents the axial velocity of the target,  $c$  represents the speed of the wave in tissue,  $B$  represents the transmitted



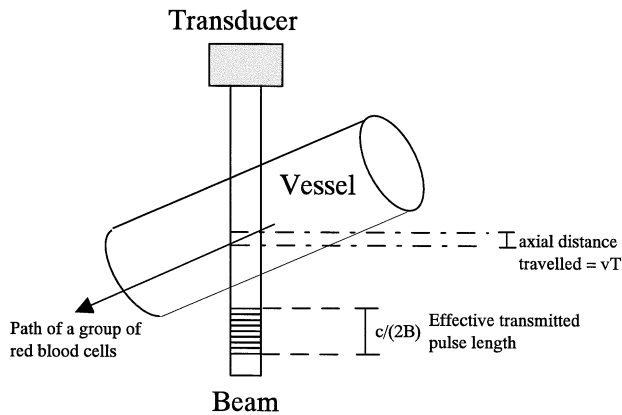


**FIGURE 65.18** Comparison of the axial distance traveled and the effective length of the transmitted pulse.

signal bandwidth, and  $T$  represents the total time interval used in estimating velocity within an individual region, then the change in delay produced by the motion of the red blood cells can be ignored [Van Trees, 1971].

This inequality is interpreted for the physical conditions of medical ultrasound in Fig. 65.18. As shown in Fig. 65.18, the value  $vT$  represents the axial distance traveled by the target while it is observed by the transducer beam, and  $c/(2B)$  represents the effective length of the signal that is used to observe the moving cells. If  $vT \ll c/(2B)$ , the shift in the position of a group of red blood cells during their travel through the ultrasonic beam is not a detectable fraction of the signal length. This leads to two important restrictions on estimation techniques. First, under the “narrowband” condition of transmission of a long (narrowband) pulse, motion of a group of cells through the beam can only be estimated using the Doppler frequency shift. Second, if the inequality is not satisfied and therefore the transmitted signal is short (wideband), faster-moving red blood cells leave the region of interest, and the use of a narrowband estimation technique produces a biased velocity estimate. Thus two strategies can be used to estimate velocity. A long (narrowband) pulse can be transmitted, and the signal from a fixed depth then can be used to estimate velocity. Alternatively, a short (wideband) signal can be transmitted in order to improve spatial resolution, and the estimator used to determine the velocity must move along with the red blood cells.

The inequality is now evaluated for typical parameters. When the angle between the axis of the beam and the axis of the vessel is 45 degrees, the axial distance traveled by the red blood cells while they cross the beam is equivalent to the lateral beam width. Using an axial distance  $vT$  of 0.75 mm, which is a reasonable lateral beam width, and an acoustic velocity of 1540 m/s, the bandwidth of the transmitted pulse must be much less than 1.026 MHz for the narrowband approximation to be valid.

Due to practical advantages in the implementation of the smaller bandwidth required by baseband signals, the center frequency of the signal is often removed before velocity estimation. The processing required for the extraction of the baseband signal is shown in Fig. 65.19. The returned signal from the transducer is amplified and coherently demodulated, through multiplication by the carrier frequency, and then a low-pass filter is applied to remove the signal sideband frequencies and noise. The remaining signal is the complex envelope. A high-pass filter is then applied to the signal from each fixed depth to remove the unwanted echoes from stationary tissue. The output of this processing is denoted as  $I_k(t)$  for the in-phase signal from the  $k$ th pulse as a function of time and  $Q_k(t)$  for the quadrature signal from the  $k$ th pulse.

## Narrowband Estimation

Narrowband estimation techniques that estimate velocity for blood at a fixed depth are described in this subsection. Both the classic Doppler technique, which frequently is used in single-sample volume systems,

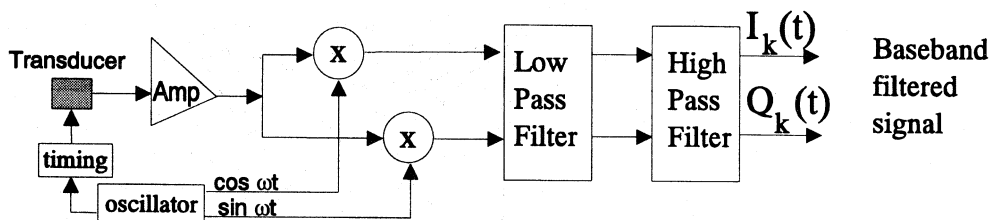


**FIGURE 65.19** Block diagram of the system architecture required to generate the baseband signal used by several estimation techniques.

and the autocorrelator, which frequently is used in color flow mapping systems, are included, as well as a finite derivative estimator and an autoregressive estimator, which have been the subject of previous research. The autocorrelator is used in real-time color flow mapping systems due to the ease of implementation and the relatively small bias and variance.

**Classic Doppler Estimation.** If the carrier frequency is removed by coherently demodulating the signal, the change in delay of the RF signal becomes a change in the phase of the baseband signal. The Doppler shift frequency from a moving target equals  $2f_c v/c$ . With a center frequency of 5 MHz, sound velocity of 1540 m/s, and blood velocity of 1 m/s, the resulting frequency shift is 6493.5 Hz. For the estimation of blood velocity, the Doppler shift is not detectable using a single short pulse, and therefore, the signal from a fixed depth and a train of pulses is acquired.

A pulse-echo Doppler processing block diagram is shown in Fig. 65.20. The baseband signal, from Figure 65.19, is shown as the input to this processing block. The received signal from each pulse is multiplied by a time window that is typically equal to the length of the transmitted pulse and integrated to produce a single data sample from each pulse. The set of data samples from a train of pulses is then Fourier-transformed, with the resulting frequency spectrum related to the axial velocity using the Doppler relationship.

Estimation of velocity using the Fourier transform of the signal from a fixed depth suffers from the limitations of all narrowband estimators, in that the variance of the estimate increases when a short pulse is transmitted. In addition, the velocity resolution produced using the Fourier transform is inversely proportional to the length of the data window. Therefore, if 64 pulses with a pulse repetition frequency of 5 kHz are used in the spectral estimate, the frequency resolution is on the order of 78.125 Hz ( $5000/64$ ). The velocity resolution for a carrier frequency of 5 MHz and speed of sound of 1540 m/s is then on the order of 1.2 cm/s, determined from the Doppler relationship. Increasing the data window only improves the velocity resolution if the majority of the red blood cells have not left the sample volume and the flow conditions have not produced a decorrelation of the signal. It is this relationship between the data window and velocity resolution, a fundamental feature of Fourier transform techniques, that has motivated the use of autoregressive estimators. The frequency and velocity resolution are not fundamentally constrained by the data window using these modern spectral estimators introduced below.

**Autoregressive Estimation (AR).** In addition to the classic techniques discussed previously, higher-order modern spectral estimation techniques have been used in an attempt to improve the velocity

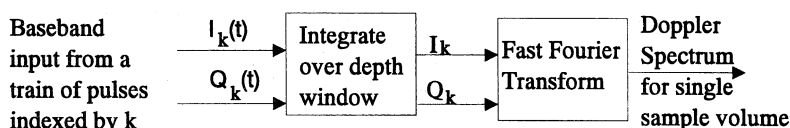


**FIGURE 65.20** Block diagram of the system architecture required to estimate the Doppler spectrum from a set of baseband samples from a fixed depth.

resolution of the estimate. These techniques are again narrowband estimation techniques, since the data samples used in computing the estimate are obtained from a fixed depth. The challenges encountered in applying such techniques to blood velocity estimation include the selection of an appropriate order which adequately models the data sequence while providing the opportunity for real-time velocity estimation and determination of the length of the data sequence to be used in the estimation process.

The goal in autoregressive velocity estimation is to model the frequency content of the received signal by a set of coefficients which could be used to reconstruct the signal spectrum. The coefficients  $a(m)$  represent the AR parameters of the  $AR(p)$  process, where  $p$  is the number of poles in the model for the signal. Estimation of the AR parameters has been accomplished using the Burg and Levinson-Durbin recursion methods. The spectrum  $P(f)$  is then estimated using the following equation:

$$P(f) = k \left| 1 + \sum_{m=1}^p a(m) \exp[-i2\pi mf] \right|^{-2}$$

The poles of the AR transfer function which lie within the unit circle can then be determined based on these parameters, and the velocity associated with each pole is determined by the Doppler equation.

Both autoregressive and autoregressive moving-average estimation techniques have been applied to single-sample-volume Doppler estimation. Order selection for single-sample-volume AR estimators is discussed in Kaluzinski [1989]. Second-order autoregressive estimation has been applied to color flow mapping by Loupas and McDicken [1990] and Ahn and Park [1991]. Although two poles are not sufficient to model the data sequence, the parameters of a higher-order process cannot be estimated in real time. In addition, the estimation of parameters of a higher-order process using the limited number of data points available in color flow mapping produces a large variance. Loupas and McDicken have used the two poles to model the signal returned from blood. Ahn and Park have used one pole to model the received signal from blood and the second pole to model the stationary signal from the surrounding tissue.

While AR techniques are useful in modeling the stationary tissue and blood and in providing a high-resolution estimate of multiple velocity components, several problems have been encountered in the practical application to blood velocity estimation. First, the order required to adequately model any region of the vessel can change when stationary tissue is present in the sample volume or when the range of velocity components in the sample volume increases. In addition, the performance of an AR estimate degrades rapidly in the presence of white noise, particularly with a small number of data samples.

**Autocorrelator.** Kasai et al. [1985] and Barber et al. [1985] discussed a narrowband *mean* velocity estimation structure for use in color flow mapping. The phase of the signal correlation at a lag of one transmitted period is estimated and used in an inverse tangent calculation of the estimated mean Doppler shift  $f_{\text{mean}}$  of the returned signal. A block diagram of the autocorrelator is shown in Fig. 65.21. The baseband signal is first integrated over a short depth window. The phase of the correlation at a lag of one pulse period is then estimated as the inverse tangent of the imaginary part of the correlation divided by the real part of the correlation. The estimated mean velocity  $v_{\text{mean}}$  of the scattering medium is then

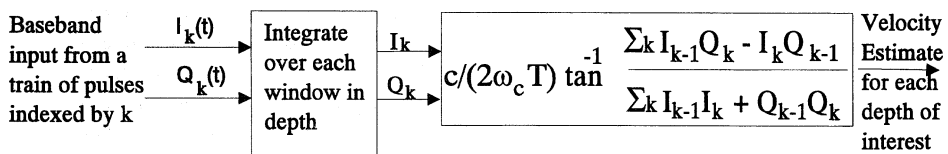


**FIGURE 65.21** Block diagram of the system architecture required to estimate the mean Doppler shift for each depth location using the autocorrelator.

determined by scaling the estimated Doppler shift by several factors, including the expected center frequency of the returned signal.

The autocorrelator structure can be derived from the definition of instantaneous frequency, from the phase of the correlation at a lag of one period, or as the first-order autoregressive estimate of the mean frequency of a baseband signal. The contributions of uncorrelated noise should average to zero in both the numerator and denominator of the autocorrelator. This is an advantage because the autocorrelation estimate is unbiased when the input signal includes the desired flow signal and noise. Alternatively, in the absence of a moving target, the input to the autocorrelator may consist only of white noise. Under these conditions, both the numerator and denominator can average to values near zero, and the resulting output of the autocorrelator has a very large variance. This estimation structure must therefore be used with a power threshold that can determine the presence or absence of a signal from blood flow and set the output of the estimator to zero when this motion is absent.

The variance of the autocorrelation estimate increases with the transmitted bandwidth, and therefore, the performance is degraded by transmitting a short pulse.

**Finite Derivative Estimator (FDE).** A second approach to mean velocity or frequency estimation is based on a finite implementation of a derivative operator. The *finite derivative* estimator is derived based on the first and second moments of the spectrum. The basis for this estimator comes from the definition of the spectral centroid:

$$v_{mean} = \frac{\int \omega S(\omega) d\omega}{\int S(\omega) d\omega} \quad (65.27)$$

The mean velocity is given by  $v_{mean}$ , which is a scaled version of the mean frequency, where the scaling constant is given by  $k'$  and  $S(\omega)$  represents the power spectral density. Letting  $R_r(\cdot)$  represent the complex signal correlation and  $\tau$  represent the difference between the two times used in the correlation estimate, Eq. (65.27) is equivalent to

$$v_{mean} = k' \frac{\left[ \frac{\partial}{\partial \tau} R_r(\tau) \right]_{\tau=0}}{R_r(0)} \quad (65.28)$$

Writing the baseband signal as the sum  $I(t) + jQ(t)$  and letting  $E$  indicate the statistical expectation, Brody and Meindl [1974] have shown that the mean velocity estimate can be rewritten as

$$v_{mean} = \frac{k' E \left\{ \frac{\partial}{\partial t} [I(t)] Q(t) - \frac{\partial}{\partial t} [Q(t)] I(t) \right\}}{E [I^2(t) + Q^2(t)]} \quad (65.29)$$

The estimate of this quantity requires estimation of the derivative of the in-phase portion  $I(t)$  and quadrature portion  $Q(t)$  of the signal. For an analog, continuous-time implementation, the bias and variance were evaluated by Brody and Meindl [1974]. The discrete case has been studied by Kristoffersen [1986]. The differentiation has been implemented in the discrete case as a finite difference or as a finite impulse response differentiation filter. The estimator is biased by noise, since the denominator represents power in the returned signal. Therefore, for nonzero noise power, the averaged noise power in the denominator will not be zero mean and will constitute a bias. The variance of the finite derivative

estimator depends on the shape and bandwidth of the Doppler spectrum, as well as on the observation interval.

### Wideband Estimation Techniques

It is desirable to transmit a short ultrasonic pulse in order to examine blood flow in small regions individually. For these short pulses, the narrowband approximation is not valid, and the estimation techniques used should track the motion of the red blood cells as they move to a new position over time. Estimation techniques that track the motion of the red blood cells are known as *wideband estimation techniques* and include cross-correlation techniques, the wideband maximum likelihood estimator and high time bandwidth estimation techniques. A thorough review of time-domain estimation techniques to estimate tissue motion is presented in Hein and O'Brien [1993].

**Cross-Correlation Estimator.** The use of time shift to estimate signal parameters has been studied extensively in radar. If the transmitted signal is known, a maximum likelihood (ML) solution for the estimation of delay has been discussed by Van Trees [1971] and others. If the signal shape is not known, the use of cross-correlation for delay estimation has been discussed by Helstrom [1968] and Knapp and Carter [1976]. If information regarding the statistics of the signal and noise are available, an MLE based on cross-correlation has been proposed by Knapp and Carter [1976] known as the *generalized correlation method for the estimation of time delay*.

Several researchers have applied cross-correlation analysis to medical ultrasound. Bonnefous and Pesque [1986], Embree and O'Brien [1986], Foster et al. [1990], and Trahey et al. [1987] have studied the estimation of mean velocity based on the change in delay due to target movement. This analysis has assumed the shape of the transmitted signal to be unknown, and a cross-correlation technique has been used to estimate the difference in delay between successive pulses. This differential delay has then been used to estimate target velocity, where the velocity estimate is now based on the change in delay of the signal over an axial window, by maximizing the cross-correlation of the returned signal over all possible target velocities. Cross-correlation processing is typically performed on the radiofrequency (RF) signal, and a typical cross-correlation block diagram is shown in Fig. 65.22. A high-pass filter is first applied to the signal from a fixed depth to remove the unwanted return from stationary tissue. One advantage of this strategy is that the variance is now inversely proportional to bandwidth of the transmitted signal rather than proportional.

**Wideband Maximum Likelihood Estimator (WMLE).** Wideband maximum likelihood estimation is a baseband strategy with performance properties that are similar to cross-correlation. The estimate of the velocity of the blood cells is jointly based on the shift in the signal envelope and the shift in the carrier frequency of the returned signal. This estimator can be derived using a model for the signal that is expected to be reflected from the moving blood medium after the signal passes through intervening tissue. The processing of the signal can be interpreted as a filter matched to the expected signal. A diagram of the processing required for the wideband maximum likelihood estimator is shown in Fig. 65.23 [Ferrara and Algazi, 1991]. Assume that  $P$  pulses were transmitted. Required processing involves the delay of the signal from the  $(P - k)$ th pulse by an amount equal to  $2v/c(kT)$ , which corresponds to the movement of the cells between pulses for a specific  $v$ , followed by multiplication by a frequency which corresponds to the expected Doppler shift frequency of the baseband returned signal. The result of this multiplication

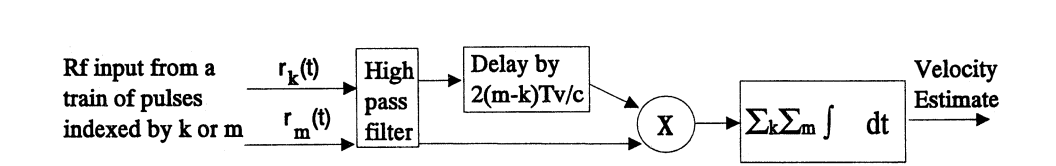


**FIGURE 65.22** Block diagram of the system architecture required to estimate the velocity at each depth using a cross-correlation estimator.

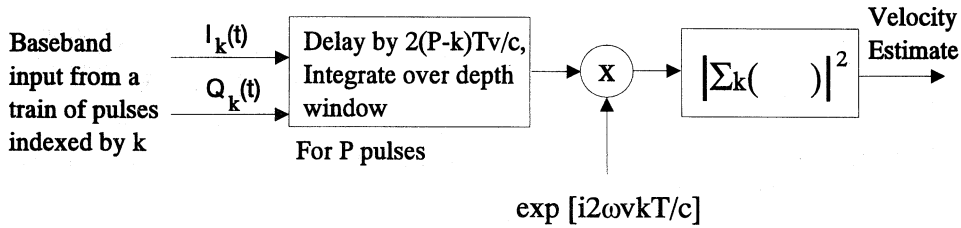


**FIGURE 65.23** Block diagram of the system architecture required to estimate the velocity at each depth using the wideband MLE.

is summed for all pulses, and the maximum likelihood velocity is then the velocity which produces the largest output from this estimator structure.

**Estimation Using High-Time-Bandwidth Signals.** Several researchers have also investigated the use of long wideband signals including “chirp” modulated signals and pseudo-random noise for the estimation of blood velocity. These signals are transmitted continuously (or with a short “flyback” time). Since these signals require continual transmission, the instantaneous power level must be reduced in order to achieve safe average power levels.

Bertram [1979] concluded that transmission of a “chirp” appears to give inferior precision for range measurement and inferior resolution of closely spaced multiple targets than a conventional pulse-echo system applied to a similar transducer. Multiple targets confuse the analysis. Using a simple sawtooth waveform, it is not possible to differentiate a stationary target at one range from a moving target at a different range. This problem could possibly be overcome with increasing and decreasing frequency intervals. Axial resolution is independent of the modulation rate, dependent only on the spectral frequency range (which is limited).

The limitations of systems that have transmitted a long pulse of random noise and correlated the return with the transmitted signal include reverberations from outside the sample volume which degrade the signal-to-noise ratio (the federally required reduction in peak transmitted power also reduces SNR), limited signal bandwidth due to frequency-dependent attenuation in tissue, and the finite transducer bandwidth [Bendick and Newhouse, 1974; Cooper and McGillem, 1972].

## New Directions

Areas of research interest, including estimation of the 3D velocity magnitude, volume flow estimation, the use of high-frequency catheter-based transducers, mapping blood flow within malignant tumors, a new display mode known as *color Doppler energy*, and the use of contrast agents, are summarized in this subsection.

**Estimation of the 3D Velocity Magnitude and Beam Vessel Angle.** Continued research designed to provide an estimate of the 3D magnitude of the flow velocity includes the use of crossed-beam Doppler systems [Overbeck et al., 1992; Wang and Yao, 1982] and tracking of speckle in two and three dimensions [Trahey et al., 1987]. Mapping of the velocity estimate in two and three dimensions, resulting in a 3D color flow map has been described by Carson et al. [1992], Picot et al. [1993], and Cosgrove et al. [1990].

**Volume Flow Estimation.** Along with the peak velocity, instantaneous velocity profile, and velocity indices, a parameter of clinical interest is the volume of flow through vessels as a function of time. Estimation strategies for the determination of the volume of flow through a vessel have been described by Embree and O’Brien [1990], Gill [1979], Hottinger and Meindl [1979], and Uematsu [1981].

**Intravascular Ultrasound.** It has been shown that intravascular ultrasonic imaging can provide information about the composition of healthy tissue and atheroma as well as anatomic data. A number of

researchers have now shown that using frequencies of 30 MHz or above, individual layers and tissue types can be differentiated [de Kroon et al., 1991a, 1991b; Lockwood et al., 1991]. Although obvious changes in the vessel wall, such as dense fibrosis and calcification, have been identified with lower-frequency transducers, more subtle changes have been difficult to detect. Recent research has indicated that the character of plaque may be a more reliable predictor of subsequent cerebrovascular symptoms than the degree of vessel narrowing or the presence of ulceration [Merritt et al., 1992]. Therefore, the recognition of subtle differences in tissue type may be extremely valuable. One signal-processing challenge in imaging the vascular wall at frequencies of 30 MHz or above is the removal of the unwanted echo from red blood cells, which is a strong interfering signal at high frequencies.

**Vascular Changes Associated with Tumors.** Three-dimensional color flow mapping of the vascular structure is proposed to provide new information for the differentiation of benign and malignant masses. Judah Folkman and associates first recognized the importance of tumor vascularity in 1971 [Folkman et al., 1971]. They hypothesized that the increased cell population required for the growth of a malignant tumor must be preceded by the production of new vessels. Subsequent work has shown that the walls of these vessels are deficient in muscular elements, and this deficiency results in a low impedance to flow [Gammill et al., 1976]. This change can be detected by an increase in diastolic flow and a change in the resistive index.

More recently, Less et al. [1991] have shown that the vascular architecture of solid mammary tumors has several distinct differences from normal tissues, at least in the microvasculature. A type of network exists that exhibits fluctuations in both the diameter and length of the vessel with increasing branch order. Current color flow mapping systems with a center frequency of 5 MHz or above have been able to detect abnormal flow with varying degrees of clinical sensitivity from 40% to 82% [Balu-Maestro et al., 1991; Belcaro et al., 1988; Luska et al., 1992]. Researchers using traditional Doppler systems have also reported a range of clinical sensitivity, with a general reporting of high sensitivity but moderate to low specificity. Burns et al., [1982] studied the signal from benign and malignant masses with 10-MHz CW Doppler. They hypothesized, and confirmed through angiography, that the tumors under study were fed by multiple small arteries, with a mean flow velocity below 10 cm/s. Carson et al. [1992] compared 10-MHz CW Doppler to 5- and 7.5-MHz color flow mapping and concluded that while 3D reconstruction of the vasculature could provide significant additional information, color flow mapping systems must increase their ability to detect slow flow in small vessels in order to effectively map the vasculature.

**Ultrasound Contrast Agents.** The introduction of substances that enhance the ultrasonic echo signal from blood primarily through the production of microbubbles is of growing interest in ultrasonic flow measurement. The increased echo power may have a significant impact in contrast echocardiography, where acquisition of the signal from the coronary arteries has been difficult. In addition, such agents have been used to increase the backscattered signal from small vessels in masses that are suspected to be malignant. Contrast agents have been developed using sonicated albumen, saccharide microbubbles, and gelatin-encapsulated microbubbles.

Research to improve the sensitivity of flow measurement systems to low-velocity flow and small volumes of flow, with the goal of mapping the vasculature architecture, includes the use of ultrasonic contrast agents with conventional Doppler signal processing [Hartley et al., 1993], as well as the detection of the second harmonic of the transducer center frequency [Shrope and Newhouse, 1993].

**Color Doppler Energy.** During 1993, a new format for the presentation of the returned signal from the blood scattering medium was introduced and termed *color Doppler energy (CDE)* or *color power imaging (CPI)*. In this format, the backscattered signal is filtered to remove the signal from stationary tissue, and the remaining energy in the backscattered signal is color encoded and displayed as an overlay on the gray-scale image. The advantage of this signal-processing technique is the sensitivity to very low flow velocities.

## Defining Terms

**Baseband signal:** The received signal after the center frequency component (carrier frequency) has been removed by demodulation.

**Carrier frequency:** The center frequency in the spectrum of the transmitted signal.

**Clutter:** An unwanted fixed signal component generated by stationary targets typically outside the region of interest (such as vessel walls).

**Complex envelope:** A signal expressed by the product of the carrier, a high-frequency component, and other lower-frequency components that comprise the envelope. The envelope is usually expressed in complex form.

**Maximum likelihood:** A statistical estimation technique that maximizes the probability of the occurrence of an event to estimate a parameter. ML estimate is the minimum variance, unbiased estimate.

## Reference

- Ahn Y, Park S. 1991. Estimation of mean frequency and variance of ultrasonic Doppler signal by using second-order autoregressive model. *IEEE Trans Ultrason Ferroelec Freq Cont* 38(3):172.
- Angelson B. 1980. Theoretical study of the scattering of ultrasound from blood. *IEEE Trans Biomed Eng* 27(2):61.
- Atkinson P, Berry MV. 1974. Random noise in ultrasonic echoes diffracted by blood. *J Phys A Math Nucl Gen* 7(11):1293.
- Balu-Maestro C, Bruneton JN, Giudicelli T, et al. 1991. Color Doppler in breast tumor pathology. *J Radiol* 72(11):579.
- Barber W, Eberhard JW, Karr S. 1985. A new time domain technique for velocity measurements using Doppler ultrasound. *IEEE Trans Biomed Eng* 32(3):213.
- Belcaro G, Laurora G, Ricci A, et al. 1988. Evaluation of flow in nodular tumors of the breast by Doppler and duplex scanning. *Acta Chir Belg* 88(5):323.
- Bertram CD. 1979. Distance resolution with the FM-CW ultrasonic echo-ranging system. *Ultrasound Med Biol* (5):61.
- Bonnefous O, Pesque P. 1986. Time domain formulation of pulse-Doppler ultrasound and blood velocity estimators by cross correlation. *Ultrasonic Imaging* 8:73.
- Brody W, Meindl J. 1974. Theoretical analysis of the CW Doppler ultrasonic flowmeter. *IEEE Trans Biomed Eng* 21(3):183.
- Burns PN, Halliwell M, Wells PNT, Webb AJ. 1982. Ultrasonic Doppler studies of the breast. *Ultrasound Med Biol* 8(2):127.
- Carson PL, Adler DD, Fowlkes JB, et al. 1992. Enhanced color flow imaging of breast cancer vasculature: continuous wave Doppler and three-dimensional display. *J Ultrasound Med* 11(8):77.
- Cosgrove DO, Bamber JC, Davey JB, et al. 1990. Color Doppler signals from breast tumors: Work in progress. *Radiology* 176(1):175.
- Curry GR, White DN. 1978. Color coded ultrasonic differential velocity arterial scanner. *Ultrasound Med Biol* 4:27.
- de Kroon MGM, Slager CJ, Gussenhoven WJ, et al. 1991. Cyclic changes of blood echogenicity in high-frequency ultrasound. *Ultrasound Med Biol* 17(7):723.
- de Kroon MGM, van der Wal LF, Gussenhoven WJ, et al. 1991. Backscatter directivity and integrated backscatter power of arterial tissue. *Int J Cardiac Imaging* 6:265.
- Embree PM, O'Brien WD Jr. 1990. Volumetric blood flow via time-domain correlation: Experimental verification. *IEEE Trans Ultrason Ferroelec Freq Cont* 37(3):176.
- Ferrara KW, Algazi VR. 1994a. A statistical analysis of the received signal from blood during laminar flow. *IEEE Trans Ultrason Ferroelec Freq Cont* 41(2):185.



- Ferrara KW, Algazi VR. 1994*b*. A theoretical and experimental analysis of the received signal from disturbed blood flow. *IEEE Trans Ultrason Ferroelec Freq Cont* 41(2):172.
- Ferrara KW, Algazi VR. 1991. A new wideband spread target maximum likelihood estimator for blood velocity estimation: I. Theory. *IEEE Trans Ultrason Ferroelec Freq Cont* 38(1):1.
- Folkman J, Nerler E, Abernathy C, Williams G. 1971. Isolation of a tumor factor responsible for angiogenesis. *J Exp Med* 33:275.
- Foster SG, Embree PM, O'Brien WD Jr. 1990. Flow velocity profile via time-domain correlation: Error analysis and computer simulation. *IEEE Trans Ultrason Ferroelec Freq Cont* 37(3):164.
- Gammill SL, Stapkey KB, Himmellarb EH. 1976. Roenigenology—Pathology correlative study of neovascularay. *AJR* 126:376.
- Gill RW. 1979. Pulsed Doppler with B-mode imaging for quantitative blood flow measurement. *Ultrasound Med Biol* 5:223.
- Hartley CJ, Cheirif J, Collier KR, Bravenec JS. 1993. Doppler quantification of echo-contrast injections in vivo. *Ultrasound Med Biol* 19(4):269.
- Hatle L, Angelsen B. 1985. *Doppler Ultrasound in Cardiology*, 3d ed. Philadelphia, Lea and Febiger.
- Hatsukami TS, Primozich J, Zierler RE, Strandness DE. 1992. Color Doppler characteristics in normal lower extremity arteries. *Ultrasound Med Biol* 18(2):167.
- Hein I, O'Brien W. 1993. Current time domain methods for assessing tissue motion. *IEEE Trans Ultrason Ferroelec Freq Cont* 40(2):84.
- Helstrom CW. 1968. *Statistical Theory of Signal Detection*. London, Pergamon Press.
- Hinze JO. 1975. *Turbulence*. New York, McGraw-Hill.
- Hottinger CF, Meindl JD. 1979. Blood flow measurement using the attenuation compensated volume flowmeter. *Ultrasonic Imaging* (1)1:1.
- Kaluzinski K. 1989. Order selection in Doppler blood flow signal spectral analysis using autoregressive modelling. *Med Biol Eng Com* 27:89.
- Kasai C, Namekawa K, Koyano A, Omoto R. 1985. Real-time two-dimensional blood flow imaging using an autocorrelation technique. *IEEE Trans Sonics Ultrason* 32(3).
- Kay S, Marple SL. 1981. Spectrum analysis. A modern perspective. *Proc IEEE* 69(11):1380.
- Kennedy RS. 1969. *Fading Dispersive Channel Theory*. New York, Wiley Interscience.
- Knapp CH, Carter GC. 1976. The generalized correlation method for estimation of time delay. *IEEE Trans Acoustics Speech Signal Proc* 24(4):320.
- Kristoffersen K, Angelsen BJ. 1985. A comparison between mean frequency estimators for multigated Doppler systems with serial signal processing. *IEEE Trans Biomed Eng* 32(9):645.
- Less JR, Skalak TC, Sevic EM, Jain RK. 1991. Microvascular architecture in a mammary carcinoma: Branching patterns and vessel dimensions. *Cancer Res* 51(1):265.
- Lockwood GR, Ryan LK, Hunt JW, Foster FS. 1991. Measurement of the ultrasonic properties of vascular tissues and blood from 35–65 MHz. *Ultrasound Med Biol* 17(7):653.
- Loupas T, McDicken WN. 1990. Low-order AR models for mean and maximum frequency estimation in the context of Doppler color flow mapping. *IEEE Trans Ultrason Ferroelec Freq Cont* 37(6):590.
- Luska G, Lott D, Risch U, von Boetticher H. 1992. The findings of color Doppler sonography in breast tumors. *Rofo Forts auf dem Gebiete der Rontgens und der Neuen Bildg Verf* 156(2):142.
- Merritt C, Bluth E. 1992. The future of carotid sonography. *AJR* 158:37.
- Mo L, Cobbold R. 1986. A stochastic model of the backscattered Doppler ultrasound from blood. *IEEE Trans Biomed Eng* 33(1):20.
- Nerem RM. 1985. Fluid dynamic considerations in the application of ultrasound flowmetry. In SA Altobelli, WF Voyles, ER Greene (eds), *Cardiovascular Ultrasonic Flowmetry*. New York, Elsevier.
- Nichols WW, O'Rourke MF. 1990. *McDonald's Blood Flow in Arteries: Theoretic, Experimental and Clinical principles*. Philadelphia, Lea and Febiger.
- Nowicki A, Reid JM. 1981. An infinite gate pulse Doppler. *Ultrasound Med Biol* 7:1.
- Overbeck JR, Beach KW, Strandness DE Jr. 1992. Vector Doppler: Accurate measurement of blood velocity in two dimensions. *Ultrasound Med Biol* 18(1):19.

- Picot PA, Rickey DW, Mitchell R, et al. 1993. Three dimensional color Doppler mapping. *Ultrasound Med Biol* 19(2):95.
- Price R. 1968. Detectors for radar astronomy. In J Evans, T Hagfors (eds), *Radar Astronomy*. New York, McGraw-Hill.
- Schrope BA, Newhouse VL. 1993. Second harmonic ultrasound blood perfusion measurement. *Ultrasound Med Biol* 19(7):567.
- Shung KK, Sigelman RA, Reid JM. 1976. Scattering of ultrasound by blood. *IEEE Trans Biomed Eng* 23(6):460.
- Shung KK, Cloutier G, Lim CC. 1992. The effects of hematocrit, shear rate, and turbulence on ultrasonic Doppler spectrum from blood. *IEEE Trans Biomed Eng* 39(5):462.
- Trahey GE, Allison JW, Von Ramm OT. 1987. Angle independent ultrasonic detection of blood flow. *IEEE Trans Biomed Eng* 34(12):964.
- Uematsu S. 1981. Determination of volume of arterial blood flow by an ultrasonic device. *J Clin Ultrason* 9:209.
- Van Trees HL. 1971. *Detection, Estimation and Modulation Theory, Part III*. New York, Wiley.
- Wang W, Yao L. 1982. A double beam Doppler ultrasound method for quantitative blood flow velocity measurement. *Ultrasound Med Biol* (8):421.
- Wells PNT. 1977. *Biomedical Ultrasonics*. London, Academic Press.

## Further Information

The bimonthly journal *IEEE Transactions on Ultrasonics Ferroelectrics and Frequency Control* reports engineering advances in the area of ultrasonic flow measurement. For subscription information, contact IEEE Service Center, 445 Hoes Lane, P.O. Box 1331, Piscataway, NJ 08855-1331. Phone (800) 678-IEEE. The journal and the yearly conference proceedings of the IEEE Ultrasonic Symposium are published by the IEEE Ultrasonic Ferroelectrics and Frequency Control Society. Membership information can be obtained from the IEEE address above or from K. Ferrara, Riverside Research Institute, 330 West 42nd Street, New York, NY 10036.

The journal *Ultrasound in Medicine and Biology*, published 10 times per year, includes new developments in ultrasound signal processing and the clinical application of these developments. For subscription information, contact Pergamon Press, Inc., 660 White Plains Road, Tarrytown, NY 10591-5153. The American Institute of Ultrasound Medicine sponsors a yearly meeting which reviews new developments in ultrasound instrumentation and the clinical applications. For information, please contact American Institute of Ultrasound in Medicine, 11200 Rockville Pike, Suite 205, Rockville, MD 20852-3139; phone: (800) 638-5352.